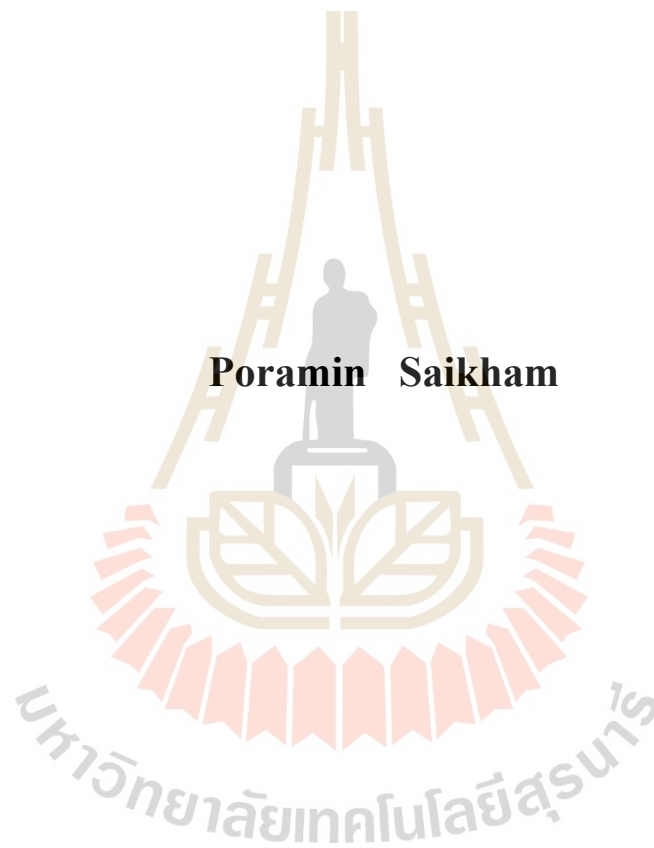


**CUMULANTS C_n OF THE CHIRAL ORDER
PARAMETER IN A NONEQUILIBRIUM CHIRAL
BJORKEN MODEL NEAR THE QCD CRITICAL POINT**



A Thesis Submitted in Partial Fulfillment of the Requirement for the

Degree of Master of Science in Physics

Suranaree University of Technology

Academic Year 2020

คู่มือแผ่นที่ C_n ของพารามิเตอร์อันดับไครเรลในแบบจำลองไครเรลย็อคเคน
ที่ไม่สมดุลบรีเวณใกล้จุดวิกฤต QCD



วิทยานิพนธ์นี้เป็นส่วนหนึ่งของการศึกษาตามหลักสูตรปริญญาวิทยาศาสตรมหาบัณฑิต
สาขาวิชาฟิสิกส์
มหาวิทยาลัยเทคโนโลยีสุรนารี
ปีการศึกษา 2563

**CUMULANTS C_n OF THE CHIRAL ORDER PARAMETER IN A
NONEQUILIBRIUM CHIRAL BJORKEN MODEL NEAR THE QCD
CRITICAL POINT**

Suranaree University of Technology has approved this thesis submitted in partial fulfillment of the requirements for a Master's Degree.

Thesis Examining Committee



(Prof. Dr. Yupeng Yan)

Chairperson



(Asst. Prof. Dr. Christoph Herold)

Member (Thesis Advisor)



(Assoc. Prof. Dr. Ayut Limphirat)

Member



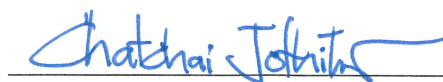
(Asst. Prof. Dr. Chinorat Kobdaj)

Member



(Dr. Jan Steinheimer)

Member



(Assoc. Prof. Dr. Chatchai Jothityangkoon)

Vice Rector for Academic Affairs
and Quality Assurance



(Prof. Dr. Santi Maensiri)

Dean of Institute of Science

ปรมินทร์ สายคำ : คummulant C_n ของพารามิเตอร์อันดับไครัลในแบบจำลองไครัล
ย็อคเคนที่ไม่สมดุลบริเวณใกล้จุดวิกฤต QCD (CUMULANTS C_n OF THE CHIRAL
ORDER PARAMETER IN A NONEQUILIBRIUM CHIRAL BJORKEN MODEL
NEAR THE QCD CRITICAL POINT) อาจารย์ที่ปรึกษา : ผู้ช่วยศาสตราจารย์ ดร.
คริสตอฟ เฮโรลด์, 90 หน้า.

เพื่อทำความเข้าใจคummulant ของจำนวนโปรตอนสุทธิที่ได้จากการทดลองในการค้นหาจุด
วิกฤตของ QCD เราจึงศึกษาแบบจำลองไดนามิกโดยอิงจากลากรองจ์เขียนควาร์ก-เมซอนที่มี
ประสิทธิภาพซึ่งมีสมมาตรไครัล งานวิจัยนี้ตรวจสอบวิวัฒนาการของตัวกลางขยายที่สร้างขึ้นใน
การชนกันของไอออนหนักโดยใช้ของไหลที่เป็นเนื้อเดียวกันเชิงพื้นที่และพารามิเตอร์ลำดับที่
ขึ้นกับเวลา สนามชิกมาที่วิวัฒนาการโดยสมการแลงเจวิน งานวิจัยแยกคummulant ของสนามชิกมา
ตามเส้นโค้งการเยือกแข็งที่เป็นพารามิเตอร์ และจับคู่จุดเยือกแข็งที่ได้รับกับพลังงานลำแสงที่
สอดคล้องกัน คummulant ของสนามชิกเหล่านี้เกี่ยวข้องกับคummulant ของจำนวนสุทธิบริเวณผ่าน
การควบคู่ของชิกมา-นิวคลีออนเพื่อให้การเปรียบเทียบเชิงคุณภาพกับข้อมูลการทดลองจาก
โปรแกรมสแกนพลังงานลำแสงของ STAR สิ่งนี้พบความเบ้ที่เพิ่มขึ้นแบบโมโนโทนิกด้วยพลังงาน
ลำแสงและพฤติกรรมที่ไม่เป็นเอกเทศของเคอร์โทซที่มีประสิทธิภาพซึ่งเกิดจากการมีอยู่ของบริเวณ
วิกฤตในแบบจำลองพื้นฐาน นอกจากนี้งานนี้ยังสาธิตให้เห็นอีกว่าการมีอยู่ของบริเวณสปินโนดัล
หรือเฟสผสมรอบการเปลี่ยนเฟสของไครัลอันดับที่หนึ่งช่วยให้เกิดคummulant ช่วงกว้างที่พลังงาน
ลำแสงต่ำสุด

สาขาวิชาฟิสิกส์
ปีการศึกษา 2563

ลายมือชื่อนักศึกษา P. Sth
ลายมือชื่ออาจารย์ที่ปรึกษา A. Wulf

PORAMIN SAIKHAM : CUMULANTS C_n OF THE CHIRAL ORDER
PARAMETER IN A NONEQUILIBRIUM CHIRAL BJORKEN MODEL
NEAR THE QCD CRITICAL POINT. THESIS ADVISOR : ASST. PROF.
CHRISTOPH HEROLD, Ph.D. 90 PP.

CUMULANTS/ CHIRAL SYMMETRY/ QCD CRITICAL POINT

To understand experimentally obtained net-proton number cumulants in the search for the QCD critical point, we study a dynamical model based on an effective quark-meson Lagrangian with chiral symmetry. This research investigate the evolution of the expanding medium created in a heavy-ion collision using a spatially homogeneous fluid and a time-dependent order parameter, the sigma field evolved by a Langevin equation. This research extract cumulants of the sigma field along a parametrized freeze out curve and match the obtained freeze out points to corresponding beam energies. These cumulants are related to cumulants of the net-baryon number through the sigma-nucleon coupling to provide a qualitative comparison to experimental data from STAR's beam energy scan program. This find a skewness that is increasing monotonically with beam energy and nonmonotonic behavior of the effective kurtosis attributed to the presence of a critical region in the underlying model. This furthermore demonstrate that the presence of the spinodal or mixed phase region around the first-order chiral phase transition allows for a wide interval of cumulants at the lowest beam energies.

School of Physics

Academic Year 2020

Student's Signature



Advisor's Signature



ACKNOWLEDGEMENTS

Firstly, I would like to thank you my adviser Dr. Christoph Herold. He had introduced me to this topic, given me a lot of papers and lecture notes, and kindly answered every question I asked. He also had pointed out some theoretical physics concepts that many students may ignore and the special numerical technique, especially. He taught me heavy-ion physic and explained the subject so clearly which was very useful for this project.

I am also appreciate to thanks to Prof. Dr. Yupeng Yan and Asst. Prof. Dr. Chinorat Kobdaj who teach me valuable knowledge. He allows me to join the particle physics group at SUT. He taught us how to write up the report and kindly checked that everything was in order. Without His precious support, it would not be possible to accomplish this thesis.

I would also like to thank my friends for their support and encouragement to keep up with the thesis. I thank Mr. Apiwit Kittiratpattana helped me with code program and gave me background information about my work.

My success for this work could not be accomplished without all of my teachers who had given me background knowledge used in my task. Moreover, I would like to thank the School of Physics, Suranaree University of Technology, and the Development and Promotion of Science and Technology Talents (DPST) Project for their scholarship.

To my family, I will not be this stronger without my parents and my sister as inspiration. I am greatly indebted to their love and kind support, the most wonderful gift one can ever ask for.

Poramin Saikham

CONTENTS

	Page
ABSTRACT IN THAI	I
ABSTRACT IN ENGLISH	II
ACKNOWLEDGEMENTS	III
CONTENTS	IV
LIST OF FIGURES	VI
CHAPTER	
I INTRODUCTION	1
II QUARK-GLUON-PLASMA AND QCD PHASE TRANSITION	4
2.1 The standard model	4
2.2 Basics of quantum field theory	6
2.2.1 Symmetries	8
2.3 Chiral Symmetry	10
2.3.1 The spontaneous symmetry breaking	13
2.3.2 Linear sigma-model	16
2.3.3 Chiral Explicit Breaking of chiral symmetry.	19
2.3.4 Chiral phase transition	22
III MODEL DESCRIPTION	26
3.1 Heavy-ion collision	26
3.2 Relativistic Hydrodynamics	28
3.2.1 Perfect fluid	29
3.2.2 Bjorken's scaling solution	31
3.3 Effective model	34

CONTENTS (Continued)

	Page
IV RESEARCH METHODOLOGY	36
4.1 Phase transition	36
4.2 Numerical evolution of sigma field	39
4.3 Numerics of hydrodynamic evolution	42
4.4 Central moment and Cumulants	44
4.4.1 Statistical Error	49
4.5 Relation of initial condition to beam energy	50
4.6 Flow diagram	51
4.6.1 Get the susceptibility of the system computed in theoretical cal- culations	51
4.6.2 Initialize Hydro and Fields	51
4.6.3 Evolve Fluid-dynamics	51
4.6.4 Cumulants	51
V RESULTS AND DISCUSSIONS	54
5.1 Chiral Phase transition	54
5.2 Freeze-out condition	56
5.3 The number of event	57
5.4 Fluctuation of sigma field	58
5.5 Fluctuation of the net-baryon number	62
5.6 Comparison with experimental data	62
VI SUMMARY AND CONCLUSIONS	66
REFERENCES	68
APPENDIX	74
CURRICULUM VITAE	79

LIST OF FIGURES

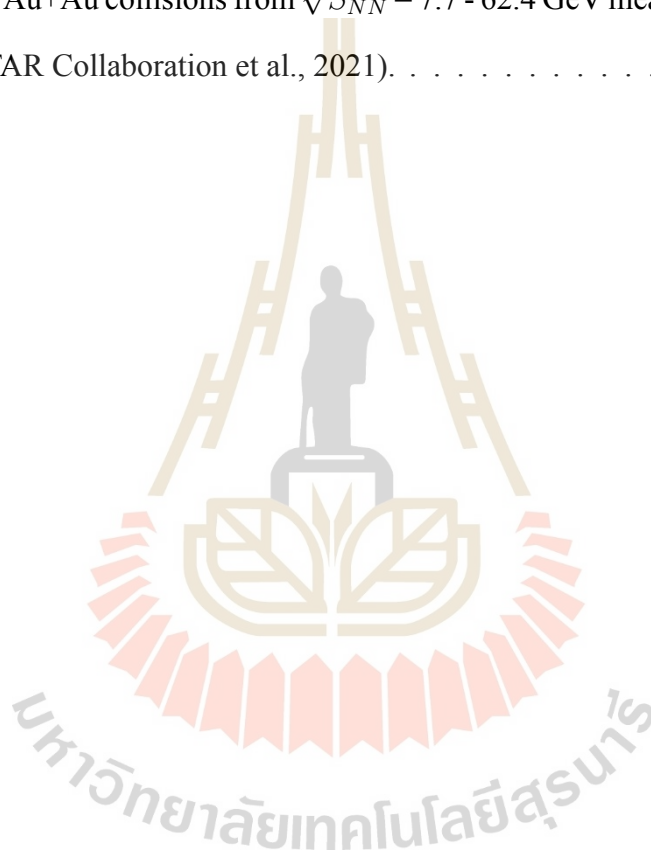
Figure		Page
2.1	The Standard Model of elementary particles, with the three generations of matter(quarks and leptons), gauge bosons(force carriers) in the fourth column, and the Higgs boson in the fifth (Fehling, 2008).	5
2.2	For $m^2 > 0$, we see the ground state is stable at $\phi = 0$	14
2.3	For $m^2 < 0$, we see clearly that the system have spontaneous symmetry breaking at the ground state because the system is not stable at $\phi = 0$	15
2.4	Potential of linear sigma-model with explicit symmetry breaking, if the explicit symmetry breaking term ϵ is close to zero we have the parameters of this model chosen as $f_\pi = 93$ MeV, $m_\pi = 138$ MeV. For finite quark mass, the explicit symmetry breaking term is $\epsilon = f_\pi m_\pi^2$	21
2.5	The sketch of phase diagram of strongly-interacting matter of confinement and de-confinement state as a function of temperature T (MeV) and baryon chemical potential μ_B (Sinha, 2016).	22
3.1	(a). Two heavy ion - flattened into a pancake shape since they are traveling near the speed of light - collide into each other. (b). Protons and neutrons dissolve for a brief instant, liberating their constituents (quarks and gluons) to form a Quark-Gluon-Plasma (very hot and dense fireball) (c). The Quark-Gluon-Plasma subsequently decays into thousands of particles (d). Each of these particles provides an information as a foot-print to what occurred inside the collision zone. https://sciencenode.org/feature/modeling-heavy-ion-collisions-open-science-grid.php	27

LIST OF FIGURES (Continued)

Figure		Page
3.2	The hadron yield ratios with best fit at the SPS beam energy of 17.3 AGeV and the RHIC $\sqrt{s} = 200$ AGeV, Figure from (Andronic et al., 2006).	29
3.3	The space-time evolution of a heavy-ion collision according to the Bjorken model (Shi et al., 2009).	32
4.1	The sigma equilibrium at all Temperature T and chemical potential μ space as shown in 3D-plot	39
4.2	The phase structure of chiral phase transition in temperature and quark chemical potential space (T, μ) . It has 3 types of the transition. The chiral first order phase transition ends at (100, 200) MeV. After this critical end point, lies a cross-over region.	40
4.3	We solve the evolution of a fireball by simulation as shown in the flow diagram calculating cumulants of σ	52
5.1	The phase structure of chiral phase transition in different initial conditions (T_{int}, μ_{int}) alongside trajectory of fireball.	55
5.2	The energy dependence of temperature T and quark chemical potential μ_q	57
5.3	The phase structure of chiral phase transition for freeze-out condition is labelled dotted-line.	58
5.4	σ^2 , $S\sigma$ and $\kappa\sigma^2$ as a function of initial condition of baryochemical potential μ_B . The different colored labelled as the different number of event.	59
5.5	σ^2 (a), $S\sigma$ (b) and $\kappa\sigma^2$ (c) of the sigma field as a function of beam energy \sqrt{s}	61

LIST OF FIGURES (Continued)

Figure		Page
5.6	The fluctuation of net-proton is shown in ratio of high moment such σ^2 , $S\sigma$ and $\kappa\sigma^2$ as a function of center of mass energy \sqrt{s}	63
5.7	(1) σ^2/M , (2) $S\sigma$ and (3) $\kappa\sigma^2$ of net-proton distributions for 0-5% central Au+Au collisions from $\sqrt{S_{NN}} = 7.7 - 62.4$ GeV measured by STAR (STAR Collaboration et al., 2021).	64



CHAPTER I

INTRODUCTION

Quark–gluon plasma (QGP) is a new state of matter that was present at extremely high temperatures and densities in the early universe. Contrary to a hadronic medium (protons, neutrons, pions, etc.), it is characterized by deconfinement and chiral symmetry restoration. In the year 2000, evidence for the new state of matter in Pb + Pb collisions was found at CERN (Conseil Européen pour la Recherche Nucléaire, Geneva, Switzerland) from the heavy-ion program at the Super Proton Synchrotron (SPS) (Schmidt et al., 1992).

The study of heavy ion collisions aims to explore the phase structure of nuclear matter as a function of baryochemical potential μ_B and temperature T (M. Stephanov et al., 1998; Alford et al., 1998). At $\mu_B = 0$, a smooth crossover has been found while for large μ_B , a discontinuous first-order phase transition is widely expected which ends at a second-order critical point (CP) (Aoki et al., 2006; Steinbrecher, 2019).

Event-by-event fluctuations of conserved quantities such as net-baryon, net-charge, and net-strangeness are sensitive to the correlation length and connected proxy to thermodynamic susceptibilities calculated in lattice QCD (Cheng et al., 2009; Gavai et al., 2008) or effective model calculations. The fluctuations of conserved quantities are defined in the form of cumulants. To compare with the experimental data, ratios of baryon number susceptibilities are used to eliminate the dependence on volume and temperature of the system which are notoriously difficult to access. Higher order cumulants of conserved quantities depend directly on higher powers of the correlation length (M. A. Stephanov, 2011), and the correlation length of the nonequilibrium system depends on expansion time and is limited by the system size. It has previously been shown

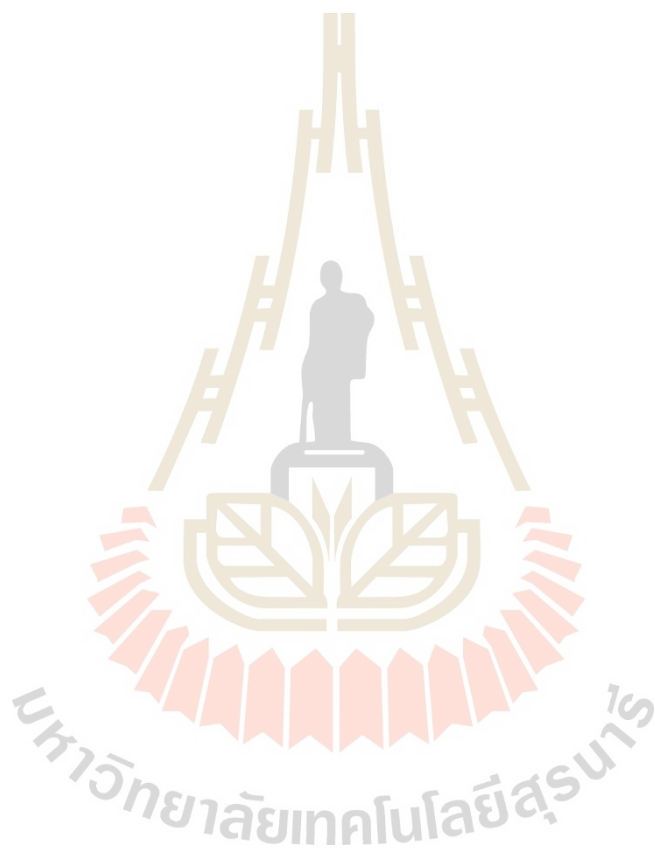
that the correlation length increases to about 2 – 3 fm near the CP (M. A. Stephanov, 2009). Experimental programs such as the beam-energy scan program of the Relativistic Heavy Ion Collider (RHIC) try to measure how e.g. net-proton skewness and kurtosis deviate from baseline calculations with e.g. UrQMD or a hadron resonance gas model to locate the QCD CP (Aggarwal et al., 2010).

The experimental data, the ratios of baryon number susceptibilities are used as $\kappa\sigma^2 = \chi_B^{(4)}/\chi_B^{(2)}$ and $S\sigma = \chi_B^{(3)}/\chi_B^{(2)}$ to ignore the volume and temperature of the system that are hard to determine. Besides, the higher order cumulants of conserved quantities depend directly on higher powers of the correlation length (M. A. Stephanov, 2011), such as $C_2 \sim \xi^2$, $C_3 \sim \xi^{4.5}$ and $C_4 \sim \xi^7$ and the correlation length of the system depends on expansion time and is limited by the system size. The correlation length increases to about 2-3 fm near the critical point (M. A. Stephanov, 2009).

Various experimental programs then try to measure how e.g. net-proton skewness and kurtosis deviate from baseline calculations with e.g. UrQMD or a hadron resonance gas model to locate the QCD CP. Heavy-ion physicists keep investigating the QCD phase transition to detect signals of a critical point (CP) in heavy-ion collisions. The beam-energy scan program of the Relativistic Heavy Ion Collider (RHIC), which is located at the Brookhaven National Laboratory (BNL), USA, then aims to study the QCD phase structure and to search for the QCD CP (Aggarwal et al., 2010).

We follow the thesis in "ENTROPY PRODUCTION AT THE CHIRAL PHASE TRANSITION" (Kittiratpattana, 2017). They study study the evolution of the expanding medium using a spatially homogeneous fluid and a time-dependent order parameter. The calculation is based on the Bjorken's picture along with the homogeneous expanding medium which simplifies the calculation into only one dimension (time). Finally, the dynamics of entropy can be easily obtained by thermodynamics relation. In this work, We focus on the calculation of the fluctuation of the order parameter and expand-

ing result to freeze-out condition. To compare with the observable we investigate the fluctuation in a net-proton number.



CHAPTER II

QUARK-GLUON-PLASMA AND QCD PHASE TRANSITION

In this Chapter we would like to give some background information, on quark- and gluon chiral symmetry. We have discussed the basic of quantum field theory then get equation of motion from the variation of the action vanished. We know all of the conserved quantity can get from transformation such as translation, rotation, time inverse, etc. We then test on chiral symmetry by the vector-axial transformation. We then talk about the spontaneous symmetry breaking which the mass of pion vanished called Goldstone Boson and chiral Explicitly Break to get the mass of sigma field. Next, we give the phase transition between chiral restoration and spontaneous chiral symmetry breaking. Finally we then illustrate the chiral phase transition and suggest evidence for a QCD critical endpoint.

2.1 The standard model

Standard model is named to explain the interaction of elementary particles. Currently, we classify fundamental particles into quarks and leptons as fermions. The fermions are either the blocks of matter with interaction of boson as the force carrier as shown in Figure 2.1.

The fermions are half-integer spin which obey Fermi-Dirac statistics called the exclusion principle. The fermions cannot occupy the same place at the same time. Bosons, in contrast, are have no problem occupying the same place at the same time obey Bose-Einstein statistic. Gluons, photons, and the W, Z and Higgs are all bosons.

Standard Model of Elementary Particles

three generations of matter (fermions)				
	I	II	III	
mass	$\approx 2.4 \text{ MeV}/c^2$	$\approx 1.275 \text{ GeV}/c^2$	$\approx 172.44 \text{ GeV}/c^2$	0
charge	$2/3$	$2/3$	$2/3$	0
spin	$1/2$	$1/2$	$1/2$	1
	u up	c charm	t top	g gluon
	d down	s strange	b bottom	γ photon
	e electron	μ muon	τ tau	Z Z boson
	ν_e electron neutrino	ν_μ muon neutrino	ν_τ tau neutrino	W W boson
				H Higgs

QUARKS (left side, purple and green labels)
LEPTONS (left side, green label)
GAUGE BOSONS (right side, red label)
SCALAR BOSONS (right side, yellow label)

Figure 2.1 The Standard Model of elementary particles, with the three generations of matter (quarks and leptons), gauge bosons (force carriers) in the fourth column, and the Higgs boson in the fifth (Fehling, 2008).

The carrier of the electromagnetic interaction is the photon. For weak and strong interaction, the carrier is W-Z boson and gluon, respectively.

Up to date, scientists found six flavors of quarks including up (u), down (d), charm (c), strange (s), top (t), bottom (b). The color-charge are red (r) blue (b) and green (g). When quarks are assembled into a hadron, the hadron has a higher mass due to the QCD interaction, for example, proton (uud) including two of u quarks with mass $0.003 \text{ GeV}/c^2$ and one of d quark with mass $0.003 \text{ GeV}/c^2$. The combination is equal to $(2 \times 0.003) + 0.006 = 0.012 \text{ GeV}/c^2$ or 12 MeV , but the mass of a proton is 938 MeV . This one is occurred by strong interaction such gluon, the gluon can be classified 8 types including $r\bar{g}, r\bar{b}, g\bar{r}, g\bar{b}, b\bar{r}, b\bar{g}, r\bar{r}, g\bar{g}$ and $b\bar{b}$ (the combination of previous one).

Now we can not detect free quark a gluon which is confinement state. The confinement determines quarks are never directly observed or found in isolation but colorless hadrons. At high E , which is due to asymptotic freedom, the quarks always exist

in a group and move freely when we work to separate one quark from another, the energy scale increases and the corresponding length scale decreases. The new state will occur at the high energy called quark-gluon plasma as a deconfinement state. In this work, we then study the quark a gluon by using effective theory which chiral perturbation is an approximation using effective values of Lagrangian with chiral symmetry in calculations.

2.2 Basics of quantum field theory

Here, I follow the explanation in “Aspects of chiral symmetry” (Koch, 1997). In this section we will talk about the essentials of quantum field theory, we start with the variation of the action S . This yields the equation of motion of Lagrange field theory. Then we will show how do we get the conservation for symmetry of the Lagrangian.

Let's start with what we know from classical mechanics. The variation of the action $S = \int_{t_1}^{t_2} dt L(q, \dot{q}, t)$ is equal to 0,

$$\delta S = 0 \Rightarrow \frac{d}{dt} \frac{\partial L}{\partial \dot{q}} - \frac{\partial L}{\partial q} = 0. \quad (2.1)$$

Here we are, $L = T - V$ is the Lagrange-function. If we have a field theory, the coordinates q will be replaced by the fields $\Phi(x, t)$. The velocities \dot{q} will also be replaced by the derivatives of the fields,

$$q \rightarrow \Phi(x, t), \quad (2.2)$$

$$\dot{q} \rightarrow \partial_\mu \Phi(x, t) \equiv \frac{\partial \Phi(x, t)}{\partial x^\mu}. \quad (2.3)$$

The Lagrange-function is then given by the spatial integral over the Lagrangian density,

\mathcal{L} , or Lagrangian :

$$L = \int d^3x \mathcal{L}(\Phi(x, t), \partial_\mu \Phi(x, t), t), \quad (2.4)$$

$$S = \int_{t_1}^{t_2} dt L = \int d^4x \mathcal{L}(\Phi(x, t), \partial_\mu \Phi(x, t), t). \quad (2.5)$$

To consider the the variation of the action, the fields can be written in form as

$$\Phi \rightarrow \Phi + \delta\Phi, \quad (2.6)$$

$$\partial_\mu \Phi \rightarrow \partial_\mu \Phi + \delta(\partial_\mu \Phi), \quad (2.7)$$

with

$$\delta(\partial_\mu \Phi) = \partial_\mu(\Phi + \delta\Phi) - \partial_\mu \Phi = \partial_\mu(\delta\Phi). \quad (2.8)$$

Consequently, the variation of the action becomes

$$\begin{aligned} \delta S &= \int_{t_1}^{t_2} dt \int d^3x \mathcal{L}(\Phi + \delta\Phi, \partial_\mu \Phi + \delta(\partial_\mu \Phi)) - \mathcal{L}(\Phi, \partial_\mu \Phi) \\ &= \int_{t_1}^{t_2} dt \int d^3x \left[\mathcal{L}(\Phi, \partial_\mu \Phi) + \frac{\partial \mathcal{L}}{\partial \Phi} \delta\Phi + \frac{\partial \mathcal{L}}{\partial(\partial_\mu \Phi)} \delta(\partial_\mu \Phi) \right] - \mathcal{L}(\Phi, \partial_\mu \Phi) \\ &= \int_{t_1}^{t_2} dt \int d^3x \left(\frac{\partial \mathcal{L}}{\partial \Phi} \delta\Phi + \frac{\partial \mathcal{L}}{\partial(\partial_\mu \Phi)} \partial_\mu(\delta\Phi) \right). \end{aligned} \quad (2.9)$$

Consider Einstein notation sum over index on last term,

$$\partial_\mu \left(\frac{\partial \mathcal{L}}{\partial(\partial_\mu \Phi)} (\delta\Phi) \right) = \partial_\mu \left(\frac{\partial \mathcal{L}}{\partial(\partial_\mu \Phi)} \right) (\delta\Phi) + \left(\frac{\partial \mathcal{L}}{\partial(\partial_\mu \Phi)} \right) \partial_\mu (\delta\Phi). \quad (2.10)$$

Due to $\delta\Phi = 0$ at t_1, t_2 , We then have,

$$\int_{t_1}^{t_2} dt \int d^3x \left(\partial_\mu \left(\frac{\partial \mathcal{L}}{\partial(\partial_\mu \Phi)} (\delta\Phi) \right) \right) = 0. \quad (2.11)$$

We have required that the variation of the action vanishes, then

$$0 = \delta S = \int_{t_1}^{t_2} dt \int d^3x \left(\frac{\partial \mathcal{L}}{\partial \Phi} - \partial_\mu \left(\frac{\partial \mathcal{L}}{\partial(\partial_\mu \Phi)} \right) \right) (\delta\Phi). \quad (2.12)$$

Now, we obtain the following equations of motion

$$\frac{\partial \mathcal{L}}{\partial \Phi} - \partial_\mu \left(\frac{\partial \mathcal{L}}{\partial(\partial_\mu \Phi)} \right) = 0. \quad (2.13)$$

If we have with more than one field, the fields are labelled by an additional index

$$\frac{\partial \mathcal{L}}{\partial \Phi_i} - \partial_\mu \left(\frac{\partial \mathcal{L}}{\partial(\partial_\mu \Phi_i)} \right) = 0. \quad (2.14)$$

2.2.1 Symmetries

What we know about classical mechanics is that if the Lagrange function is independent of space and time, then momentum and energy are conserved. Here in quantum field theory, the symmetries of the Lagrangian formulation lead to conserved quantities as current conservation. Let us assume that \mathcal{L} is symmetric under a transformation of the fields,

$$\Phi \longrightarrow \Phi + \delta\Phi. \quad (2.15)$$

It becomes

$$\mathcal{L}(\Phi + \delta\Phi) = \mathcal{L}(\Phi), \quad (2.16)$$

$$\Rightarrow 0 = \mathcal{L}(\Phi + \delta\Phi) - \mathcal{L}(\Phi) = \frac{\partial \mathcal{L}}{\partial \Phi} \delta\Phi + \frac{\partial \mathcal{L}}{\partial(\partial_\mu \Phi)} \delta(\partial_\mu \Phi). \quad (2.17)$$

Using eq. (2.8) and the equation of motion (2.13) we have

$$\begin{aligned} 0 &= \left(\partial_\mu \frac{\partial \mathcal{L}}{\partial \Phi} \right) \delta\Phi + \frac{\partial \mathcal{L}}{\partial(\partial_\mu \Phi)} (\partial_\mu \delta\Phi) \\ &= \partial_\mu \left(\frac{\partial \mathcal{L}}{\partial(\partial_\mu \Phi)} \delta\Phi \right). \end{aligned} \quad (2.18)$$

So that,

$$J^\mu = \frac{\partial \mathcal{L}}{\partial(\partial_\mu \Phi_i)} \delta\Phi_i. \quad (2.19)$$

This is a conserved current, with $\partial_\mu J^\mu = 0$. Let us now add a symmetry breaking term to the Lagrangian,

$$\mathcal{L} = \mathcal{L}_0 + \mathcal{L}_1. \quad (2.20)$$

Where \mathcal{L}_0 is the symmetric part and \mathcal{L}_1 is non - symmetric under (2.15). So, the variation of the Lagrangian \mathcal{L} is non - zero and becomes

$$\delta\mathcal{L} = \delta\mathcal{L}_1. \quad (2.21)$$

We have divergence of current by following,

$$\delta\mathcal{L} = \delta\mathcal{L}_1 = \partial^\mu J_\mu. \quad (2.22)$$

Since $\delta\mathcal{L}_1 \neq 0$ the current J_μ is not conserved. That means the symmetry breaking leads to non-conservation of the current.

2.3 Chiral Symmetry

Firstly, we would like to introduce the conserved ‘axial-vector’ current. For massless fermions, if its Lagrangian is invariant, this symmetry thus is called chiral symmetry. Consider the massless Dirac field which is corresponding to QCD Lagrangian with out the interaction of gluon field strength tensor and invariant under the vector - axial transformations. To investigate symmetry of massless Dirac field the Lagrangian is given by

$$\mathcal{L} = i\bar{\psi}_j \not{\partial} \psi_j, \quad (2.23)$$

where the index ‘ j ’ labels the two quark flavors ‘up’ and ‘down’.

Now, With the Pauli - (iso)spin- matrices $\vec{\tau}$ and $\psi = (u, d)$ we consider the transformation Λ_V which changes sign if rotated through 180 degree,

$$\Lambda_V : \psi \rightarrow e^{-i\frac{\vec{\tau}}{2}\vec{\Theta}}\psi \simeq (1 - i\frac{\vec{\tau}}{2}\vec{\Theta})\psi, \quad (2.24)$$

$$\bar{\psi} \rightarrow e^{+i\frac{\vec{\tau}}{2}\vec{\Theta}}\bar{\psi} \simeq (1 + i\frac{\vec{\tau}}{2}\vec{\Theta})\bar{\psi}. \quad (2.25)$$

The Lagrangian is invariant under Λ_V transformation,

$$\begin{aligned} i\bar{\psi}\not{\partial}\psi &\longrightarrow i\bar{\psi}\not{\partial}\psi - i\vec{\Theta} \left(\bar{\psi}i\not{\partial}\frac{\vec{\tau}}{2}\psi - \bar{\psi}\frac{\vec{\tau}}{2}i\not{\partial}\psi \right) \\ &= i\bar{\psi}\not{\partial}\psi. \end{aligned} \quad (2.26)$$

From the previous section eq.(2.19), the 'vector' current divided by $\vec{\Theta}$ can be written as

$$V_\mu^a = \bar{\psi}\gamma_\mu\frac{\tau^a}{2}\psi. \quad (2.27)$$

Consider another transformation, it like vector under rotation but opposite sign to vector under parity transformation :

$$\Lambda_A : \quad \psi \longrightarrow e^{-i\gamma_5\frac{\vec{\tau}}{2}\vec{\Theta}}\psi = (1 - i\gamma_5\frac{\vec{\tau}}{2}\vec{\Theta})\psi, \quad (2.28)$$

$$\Rightarrow \bar{\psi} \longrightarrow e^{-i\gamma_5\frac{\vec{\tau}}{2}\vec{\Theta}}\bar{\psi} \simeq (1 - i\gamma_5\frac{\vec{\tau}}{2}\vec{\Theta})\bar{\psi}. \quad (2.29)$$

We see the Lagrangian Eq. (2.23) is invariant by following

$$i\bar{\psi}\not{\partial}\psi \longrightarrow i\bar{\psi}\not{\partial}\psi - i\vec{\Theta} \left(\bar{\psi}i\partial_\mu\gamma^\mu\gamma_5\frac{\vec{\tau}}{2}\psi + \bar{\psi}\gamma_5\frac{\vec{\tau}}{2}i\partial_\mu\gamma^\mu\psi \right) \quad (2.30)$$

$$= i\bar{\psi}\not{\partial}\psi. \quad (2.31)$$

Then we obtain the conserved 'axial - vector' current,

$$A_\mu^a = \bar{\psi}\gamma_\mu\gamma_5\frac{\tau^a}{2}\psi. \quad (2.32)$$

Now consider a finite quark mass and apply the above transformations to,

$$\delta\mathcal{L} = -m(\bar{\psi}\psi). \quad (2.33)$$

This is invariant under the vector transformations Λ_V , under axial transformation Λ_A we get,

$$\Lambda_A : m(\bar{\psi}\psi) \longrightarrow m\bar{\psi}\psi - 2im\vec{\Theta} \left(\bar{\psi} \frac{\vec{\tau}}{2} \gamma_5 \psi \right). \quad (2.34)$$

Hence \mathcal{L} is not Λ_A invariant for finite quark masses. But as the masses are very small compared to the relevant energy scale Λ_{QCD} , Λ_A can be regarded as the symmetry. We have developed the vector-axial transformation to the combination of quark field for example pions and sigma fields we obtain,

$$\text{pion-like state: } \vec{\pi} \equiv i\bar{\psi} \vec{\tau} \gamma_5 \psi; \quad \text{sigma-like state: } \sigma \equiv \bar{\psi} \psi$$

Here we go, the vector transformation Λ_V is obtained as,

$$\begin{aligned} \pi_i : i\bar{\psi} \tau_i \gamma_5 \psi &\longrightarrow i\bar{\psi} \tau_i \gamma_5 \psi + \Theta_j \left(\bar{\psi} \tau_i \gamma_5 \frac{\tau_j}{2} \psi - \bar{\psi} \frac{\tau_j}{2} \tau_i \gamma_5 \psi \right) \\ &= i\bar{\psi} \tau_i \gamma_5 \psi + i\Theta_j \epsilon_{ijk} \bar{\psi} \gamma_5 \tau_k \psi. \end{aligned} \quad (2.35)$$

Using the commutator, $[\tau_i, \tau_j] = 2i\epsilon_{ijk}\tau_k$, we obtain the isospin rotations,

$$\vec{\pi} \longrightarrow \vec{\pi} + \vec{\Theta} \times \vec{\pi}. \quad (2.36)$$

Similarly, it is easy to see that under Λ_V ,

$$\sigma \longrightarrow \sigma. \quad (2.37)$$

The axial transformations Λ_A to test the symmetries give us,

$$\begin{aligned}\pi_i : i\bar{\psi}\tau_i\gamma_5\psi &\longrightarrow i\bar{\psi}\tau_i\gamma_5\psi + \Theta_j \left(\bar{\psi}\tau_i\gamma_5\gamma_5\frac{\tau_j}{2}\psi + \bar{\psi}\gamma_5\frac{\tau_j}{2}\tau_i\gamma_5\psi \right) \\ &= i\bar{\psi}\tau_i\gamma_5\psi + \Theta_i\bar{\psi}\psi.\end{aligned}\quad (2.38)$$

Using the anti-commutation relation of the τ , $\{\tau_i, \tau_j\} = 2\delta_{ij}$. The pi-mesons become,

$$\vec{\pi} \longrightarrow \vec{\pi} + \vec{\Theta}\sigma. \quad (2.39)$$

Similarly, we have

$$\sigma \longrightarrow \sigma - \vec{\Theta}\vec{\pi}. \quad (2.40)$$

We see the sigma field and the pions are not invariant under axial transformation, but transformation achieve from into each other (mixing). To get a Lagrangian with chiral symmetry, we have to use a suitable combination of $\sigma, \vec{\pi}$ to axial-vector invariance. We see that $\sigma^2 + \pi^2$ is a good choice because it is invariant under axial-vector transformation. We will investigate this further in next Section.

2.3.1 The spontaneous symmetry breaking

To illustrate spontaneous symmetry breaking we consider a Lagrangian for a scalar field, ϕ , in a potential V ,

$$\mathcal{L} = \partial_\mu\phi\partial^\mu\phi^* - V(\phi), \quad (2.41)$$

where $\phi = \phi_1 + i\phi_2$ and the potential energy $V(\phi)$ is given by

$$V(\phi) = m^2\phi^2 + \lambda\phi^4. \quad (2.42)$$

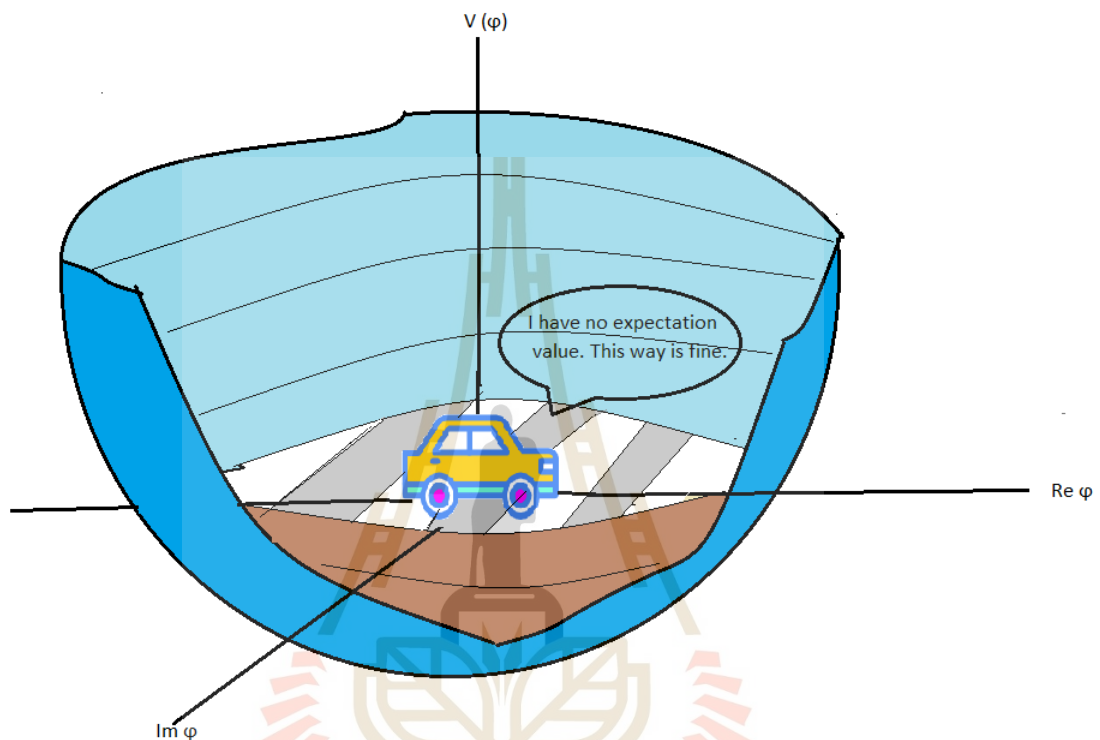


Figure 2.2 For $m^2 > 0$, we see the ground state is stable at $\phi = 0$.

In Figure 2.2 the ground state is on the middle which is a local minimum of the potential and is invariant under rotations.

In Figure 2.3, the state at $\phi = 0$ is not stable which is a local maximum of the potential. The system chooses $\phi = ae^{i\theta}$ to be ground state. We can not specific the ground state because they are degenerate ground state under radius a at any θ . If we choose some point of the ground state, it is not invaraint under rotations anymore. This is called the spontaneous symmetry breaking.

if we move the ball around in the valley, it does not cost any energy due to massless boson called Goldstone boson later. Then we will test global transformation

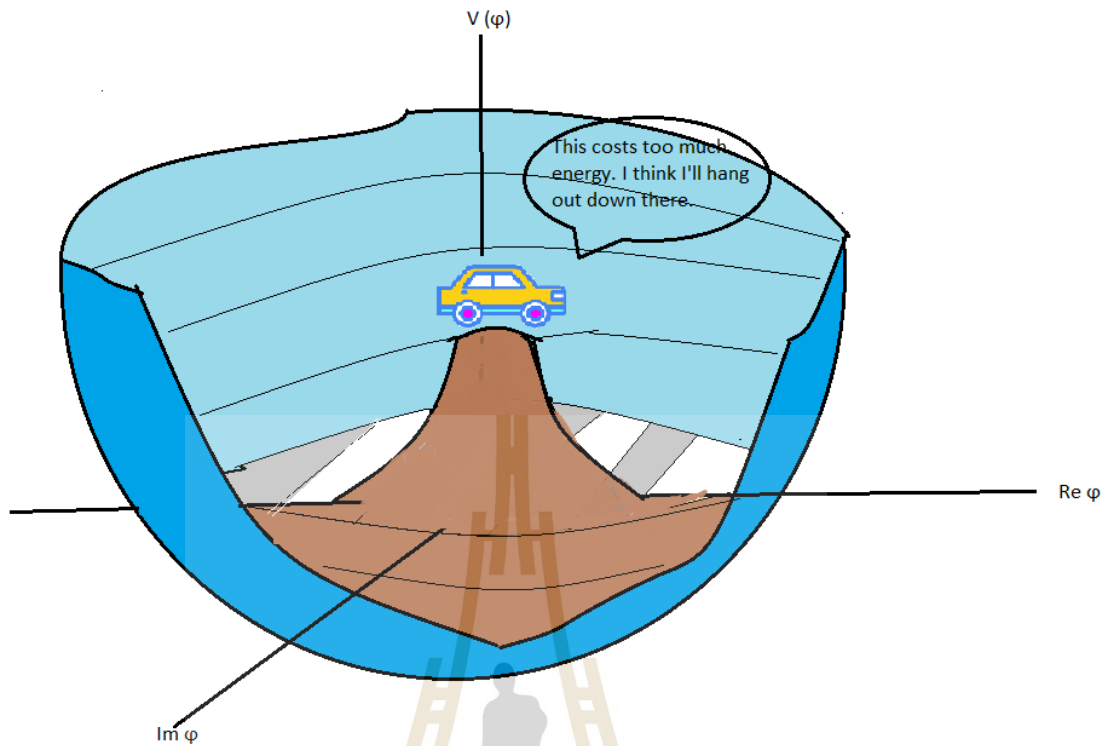


Figure 2.3 For $m^2 < 0$, we see clearly that the system have spontaneous symmetry breaking at the ground state because the system is not stable at $\phi = 0$.

U(1) of this lagrangian, consider the field in form of this formula

$$\phi = (a + \rho)e^{i\theta}. \quad (2.43)$$

The lagrangian under U(1) is given by

$$\mathcal{L} = \partial_\mu \rho \partial^\mu \rho + (\rho + a) \partial_\mu \theta \partial^\mu \theta - V(\rho), \quad (2.44)$$

and the potential is obtained as

$$V(\rho) = \lambda(\rho^4 + 4a\rho^3 + 4a^2\rho^2 - a^4). \quad (2.45)$$

Now we have the new lagrangian. For $s = 0$, we have Klein - Gordon equation and its

Lagrangian as

$$(\partial_\mu \sigma \partial^\mu \sigma + m^2) = 0, \quad (2.46)$$

$$\mathcal{L}_{KG} = \frac{1}{2} (\partial_\mu \sigma) (\partial^\mu \sigma) - \frac{1}{2} m^2 \sigma^2 \quad (2.47)$$

To find the mass of scalar field, we have to compare with Klein - Gordon. The result gives ρ field as mass = $4\lambda a^2 \rho^2$. Moreover the θ field have no mass. For strong interaction QCD, we expect to have a finite scalar quark condensate $\langle \bar{q}q \rangle \neq 0$. In this figure, it does not lose any energy in flat-direction due to a pion mass vanished which we see from the PCAC relation, but radial-direction, there are massive σ because they are moving like a harmonic oscillation with pullback force (Restoring force) due to mass. So, we obtain the different masses of the pion and sigma from breaking the symmetry. This is why π is so small compared to other hadrons.

2.3.2 Linear sigma-model

In this section, we will construct a chirally invariant Lagrangian using pions and interaction of scalar fields called linear sigma - model. Firstly, This model was suggested by Gell-Mann and Levy in 1960, the original one had nucleons.

Chiral symmetry, the Lagrangian does not change under transformations $SU(2) \times SU(2)$, Consider the following the pion and σ -field transforms under Λ_V and Λ_A give,

$$\Lambda_V : \pi_i \longrightarrow \pi_i + \epsilon_{ijk} \Theta_j \pi_k \quad \Lambda_A : \pi_i \longrightarrow \pi_i + \Theta_i \sigma \quad (2.48)$$

$$\Lambda_V : \sigma \longrightarrow \sigma \quad \Lambda_A : \sigma \longrightarrow \sigma - \Theta_i \pi_i. \quad (2.49)$$

The squares of the fields,

$$\Lambda_V : \pi^2 \longrightarrow \pi^2; \quad \sigma^2 \longrightarrow \sigma^2 \quad (2.50)$$

$$\Lambda_A : \vec{\pi}^2 \longrightarrow \vec{\pi}^2 + 2\sigma\Theta_i\pi_i; \quad \sigma^2 \longrightarrow \sigma^2 - 2\sigma\Theta_i\pi_i. \quad (2.51)$$

We see clearly that σ^2, π^2 are Λ_V invariant but not Λ_A invariant. Nevertheless, the combination $(\vec{\pi}^2 + \sigma^2)$ is invariant under both transformations, Λ_V and Λ_A ,

$$\Lambda_V, \Lambda_A : (\vec{\pi}^2 + \sigma^2) \longrightarrow (\vec{\pi}^2 + \sigma^2). \quad (2.52)$$

We now introduce further part of the Lagrangian and make sure that they are invariant under chiral symmetry transformation Λ_V, Λ_A .

The pion - quark interaction can give in the form of the combination of the quark field multiplied by pion field with normalized coupling constant g_π ,

$$g_\pi (i\bar{\psi}\gamma_5\vec{\tau}\psi) \vec{\pi}. \quad (2.53)$$

In above equation, the chiral transformations gives π^2 . To make it invariant, we have to add some term that the chiral transformations obtain σ^2 . That one is the meson-sigma interaction,

$$g_\pi (\bar{\psi}\psi) \sigma. \quad (2.54)$$

As a result, the interaction term between nucleons and the mesons is,

$$\delta\mathcal{L} = -g_\pi [(i\bar{\psi}\gamma_5\vec{\tau}\psi) \vec{\pi} + (\bar{\psi}\psi) \sigma]. \quad (2.55)$$

Next, we need to find the potential. It must be chirally invariant as a function of $V(\pi^2 + \sigma^2)$. It is often referred to as the ‘Mexican - hat - potential and its minimum at $\sigma = f_\pi$ for $\pi = 0$. The simplest form is obtained as,

$$V = V(\pi^2 + \sigma^2) = \frac{\lambda}{4} ((\pi^2 + \sigma^2) - f_\pi^2)^2. \quad (2.56)$$

From this potential behave like Figure 2.3, we found the pion to be massless corresponding to θ and the σ -meson to be massive like ρ field that it describes spontaneous symmetry breaking. Finally, we have to add kinetic energy terms for the mesons. For $s = 1/2$, we have the Dirac equation and its Lagrangian as

$$\mathcal{L}_{Dirac} = i\bar{\psi}\not{\partial}\psi. \quad (2.57)$$

For $s = 0$, we have the Klein - Gordon equation and its Lagrangian as

$$\mathcal{L}_{KG} = \frac{1}{2}(\partial_\mu\pi\partial^\mu\pi + \partial_\mu\sigma\partial^\mu\sigma). \quad (2.58)$$

All of these are part of the Lagrangian of the linear sigma-model, we combine them together as follows,

$$\begin{aligned} \mathcal{L}_{L.S.} = & i\bar{\psi}\not{\partial}\psi - g_\pi (i\bar{\psi}\gamma_5\vec{\tau}\psi\vec{\pi} + \bar{\psi}\psi\sigma) \\ & - \frac{\lambda}{4} ((\pi^2 + \sigma^2) - f_\pi^2)^2 + \frac{1}{2}\partial_\mu\pi\partial^\mu\pi + \frac{1}{2}\partial_\mu\sigma\partial^\mu\sigma. \end{aligned} \quad (2.59)$$

From the chiral potential, the spontaneous symmetry breaking chiral potential creates the massive σ -meson and massless pion. To obtain the mass of sigma, we put perturbation on the system as small fluctuation around the ground state,

$$\sigma = \sigma_0 + (\delta\sigma); \quad \pi = (\delta\pi). \quad (2.60)$$

Then we put the fluctuation on the chiral potential to linear order vanished. It gives,

$$V(\sigma, \pi) = \lambda f_\pi^2 (\delta\sigma)^2 + \mathcal{O}(\delta^3). \quad (2.61)$$

The mass of sigma is characterized by temperature and chemical potential and it is equal to the curvature of the thermodynamic potential in equilibrium,

$$m_\sigma^2 = \left. \frac{\partial^2 V}{\partial \sigma^2} \right|_{\sigma=\langle\sigma\rangle}. \quad (2.62)$$

Note that $\sigma_0 = f_\pi$, we have

$$m_\sigma^2 = 2\lambda f_\pi^2 \neq 0. \quad (2.63)$$

In summary, we have ground state characterized by,

$$\langle \sigma \rangle = \sigma_0 = f_\pi \quad (2.64)$$

$$\langle \pi \rangle = 0 \quad (2.65)$$

$$m_q = g_\pi \sigma_0 = g_\pi f_\pi \quad (2.66)$$

$$m_\sigma^2 = 2\lambda f_\pi^2 \neq 0 \quad (2.67)$$

$$m_\pi = 0. \quad (2.68)$$

2.3.3 Chiral Explicit Breaking of chiral symmetry.

In QCD we have a non zero quark mass term, leading to what is called explicit symmetry breaking,

$$\delta\mathcal{L}_{\chi SB} = -m\bar{q}q. \quad (2.69)$$

This mass term will be also considered in our linear sigma model. As shown in eq. (2.34), this term is not invariant under the axial transformation Λ_A , but it is invariant under Λ_V . We then put the explicit breaking term on the Lagrangian as following,

$$\delta\mathcal{L}_{SB} = \epsilon\sigma. \quad (2.70)$$

Here ϵ is the symmetry breaking parameter. The potential V eq. (2.56) becomes,

$$V(\sigma, \pi) = \frac{\lambda}{4} ((\pi^2 + \sigma^2) - v_0^2)^2 - \epsilon\sigma. \quad (2.71)$$

On the explicit symmetry breaking case, we have replaced f_π by a parameter v_0 for limit of $\epsilon \rightarrow 0$. From equation (2.71), the symmetry breaking term is to tilt the potential see Figure 2.4.

To find what the parameter v_0 is, the derivative of the potential with respect to scalar field σ at $\sigma_0 = f_\pi$ leading,

$$v_0 = f_\pi - \frac{\epsilon}{2\lambda f_\pi^2}. \quad (2.72)$$

The mass of the sigma is change, and now the pion mass is not massless. It becomes,

$$m_\sigma^2 = \left. \frac{\partial^2 V}{\partial \sigma^2} \right|_{\sigma_0} = 2\lambda f_\pi^2 + \frac{\epsilon}{f_\pi}, \quad (2.73)$$

$$m_\pi^2 = \left. \frac{\partial^2 V}{\partial \pi^2} \right|_{\sigma_0} = \frac{\epsilon}{f_\pi} \neq 0. \quad (2.74)$$

However the nucleon mass term should not be changed, it is the contribution of the symmetric part of the potential ($\sim v_0$) and the symmetry breaking term ($\sim \epsilon$). Using

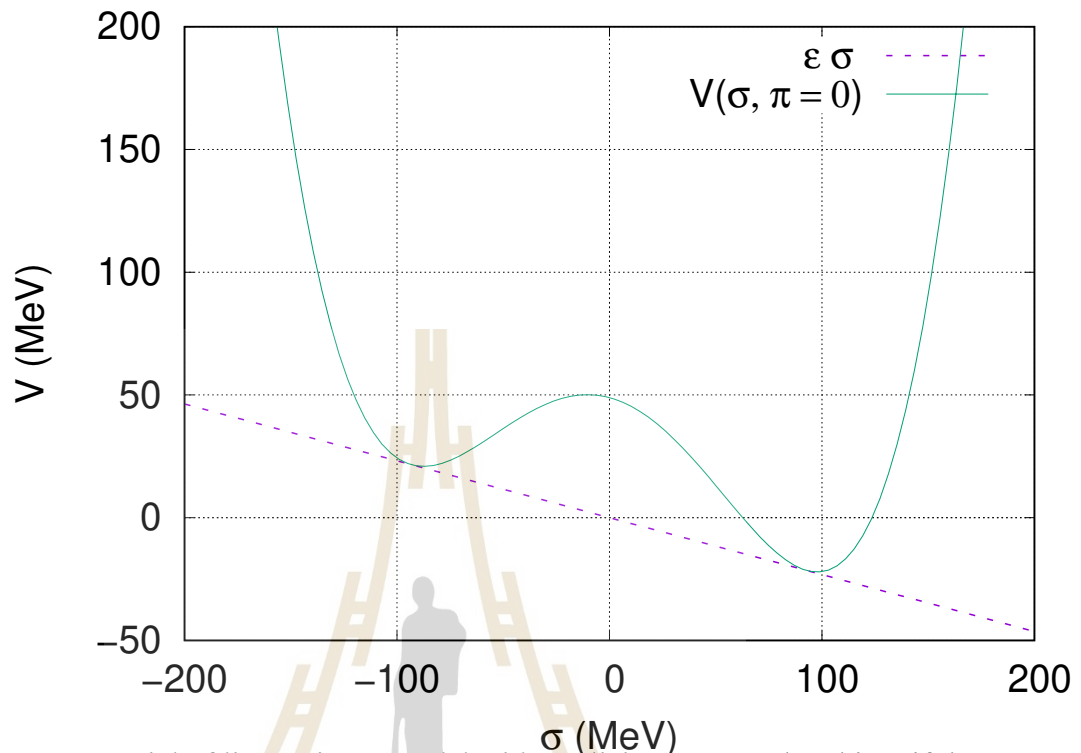


Figure 2.4 Potential of linear sigma-model with explicit symmetry breaking, if the explicit symmetry breaking term ϵ is close to zero we have the parameters of this model chosen as $f_\pi = 93$ MeV, $m_\pi = 138$ MeV. For finite quark mass, the explicit symmetry breaking term is $\epsilon = f_\pi m_\pi^2$.

the Goldberger-Treiman relation, we have

$$M_N = g_\pi \sigma_0 = g_\pi \left(v_0 + \frac{\epsilon}{2\lambda f_\pi^2} \right). \quad (2.75)$$

Substituting mass of σ and π on the above equation, we obtain

$$\Sigma_{\pi N} = \delta M_N^{X\chi SB} = g_\pi \frac{\epsilon}{2\lambda f_\pi^2} \simeq g_\pi f_\pi \frac{m_\pi^2}{m_\sigma^2}. \quad (2.76)$$

Experimentally, the pion-nucleon scattering gives (**Hoe83**) $\Sigma_{\pi N}(0) = 35 \pm 5$ MeV.

2.3.4 Chiral phase transition

We previously mentioned the spontaneous symmetry breaking in the QCD vacuum. At high temperatures or baryon densities, lattice QCD expects chiral symmetry to be restored with above a temperature $T \sim 150$ MeV that is believed to be created in nuclear collisions on the ultra-relativistic regime. To investigate the existence of chiral symmetry restoration. The bump in the potential would vanish, creating one single minimum. The pions would not behave like Goldstone bosons anymore and become massive.

In present work, we study the chiral phase transition between QGP, where the chiral symmetry is restored, and a hadronic medium, where chiral symmetry is spontaneously broken. Our goal is to study the chiral transition and to investigate the impact of a critical point at nonzero baryochemical potential μ and temperature T .

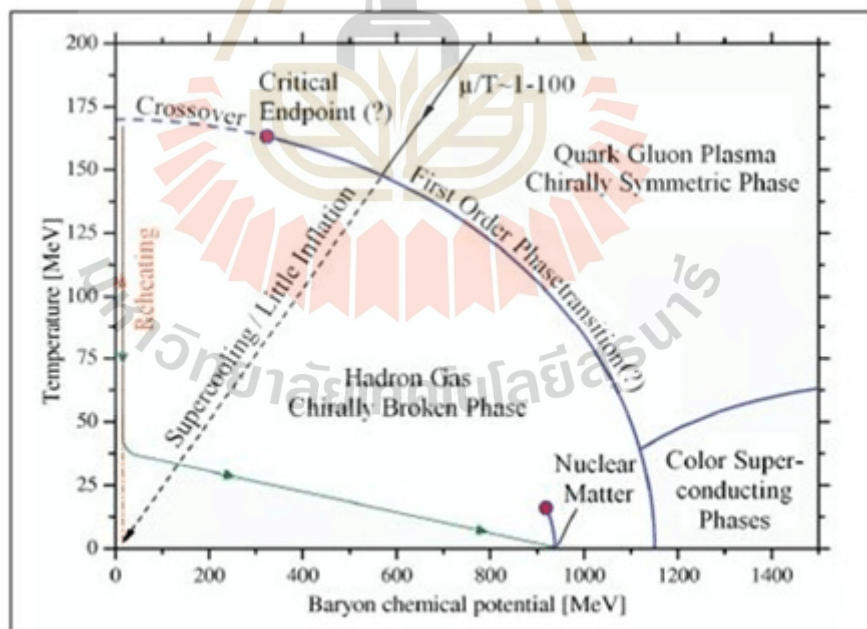


Figure 2.5 The sketch of phase diagram of strongly-interacting matter of confinement and de-confinement state as a function of temperature T (MeV) and baryon chemical potential μ_B (Sinha, 2016).

The phase transition show temperature T as a function of μ to separate a

crossover, the first-order phase transition and the second-order phase transition where the correlation length is diverge of susceptibilities. Due to the large correlation length ξ , we expect to see the critical point as the second order phase transition suggested by (M. Stephanov et al., 1998). We find that $m_\sigma = 1/\xi$ and the critical point is characterized by $\xi \rightarrow \infty$.

Such a phase structure is provided by the linear sigma model. We have the Lagrangian of the linear sigma model, following

$$\mathcal{L} = \bar{q} [i\gamma^\mu \partial_\mu - g(\sigma + i\gamma_5 \vec{\tau} \cdot \vec{\pi})] q + \frac{1}{2} (\partial_\mu \sigma \partial^\mu \sigma + \partial_\mu \vec{\pi} \cdot \partial^\mu \vec{\pi}) - U(\sigma, \vec{\pi}) . \quad (2.77)$$

Here the potential is written as

$$U(\sigma, \vec{\pi}) = \frac{\lambda^2}{4} (\sigma^2 + \vec{\pi}^2 - v^2)^2 - \epsilon \sigma . \quad (2.78)$$

The simplest way to find the boundary of phase transition is by minimizing the grand canonical potential, $\Omega(\sigma_{eq}, T, \mu)$ to find the equilibrium sigma $\langle \sigma \rangle = \sigma_{eq}$, following

$$\left. \frac{\partial \Omega(\sigma, T, \mu)}{\partial \sigma} \right|_{\sigma_{eq}} = 0. \quad (2.79)$$

Here we have a system of quarks and antiquarks in thermodynamical equilibrium at temperature T and quark chemical potential $\mu \equiv \mu_B/3$, consider the grand partition function in mean - field path integral

$$\mathcal{Z} = \text{Tr} \exp \left[- \left(\hat{\mathcal{H}} - \mu \hat{\mathcal{N}} \right) / T \right] = \int \mathcal{D}\bar{q} \mathcal{D}q \mathcal{D}\sigma \mathcal{D}\vec{\pi} \exp \left[\int_x (\mathcal{L} + \mu \bar{q} \gamma^0 q) \right] . \quad (2.80)$$

Here $\int_x \equiv i \int_0^{1/T} dt \int_V d^3\mathbf{x}$, where V is the volume of the system.

The grand canonical potential given by integrating the quark degrees of freedom

in the path integral formulation of the grand canonical partition function becomes

$$\Omega(T, \mu) = -\frac{T \ln \mathcal{Z}}{V} = U(\sigma, \vec{\pi}) + \Omega_{q\bar{q}}. \quad (2.81)$$

In above equation, the potential of quark and antiquark contribution is given by

$$\Omega_{q\bar{q}} = -2N_c N_f T \int \frac{d^3 \mathbf{p}}{(2\pi)^3} \left\{ \ln \left[1 + \exp \left(\frac{E - \mu}{T} \right) \right] + \ln \left[1 + \exp \left(\frac{E + \mu}{T} \right) \right] \right\}. \quad (2.82)$$

Here the number of degrees of freedom for quarks is equal to $2N_c N_f = 12$ for 2 flavor (u,d) and 3 colours. Likewise, the relativistic energy of the valence quark and antiquark under ultra-relativistic, $E = \sqrt{p^2 + m_q^2}$, $m_q = g\sigma$.

We have the grand canonical potential, we can obtain to any other thermodynamics quantities by,

$$\Omega = e - Ts - \mu n = -p \quad (2.83)$$

$$= e - T \left(\frac{\partial p}{\partial T} \right) - \mu \left(\frac{\partial p}{\partial \mu} \right). \quad (2.84)$$

The distribution of quark n_q and anti-quark $n_{\bar{q}}$ function can be written as

$$n_q(T, \mu) = \frac{1}{1 + \exp[(E - \mu)/T]}, \quad n_{\bar{q}}(T, \mu) = n_q(T, -\mu). \quad (2.85)$$

The nucleon is composed of 3 constituent quarks. The net quark density is then obviously $n = 3n_B$. The baryon-chemical potential has required the quark and anti-

quark distribution

$$n_B = -\frac{1}{3} \frac{\partial \Omega}{\partial \mu} = \frac{\nu_q}{6\pi^2} \int p^2 dp [n_q(T, \mu) - n_{\bar{q}}(T, \mu)]. \quad (2.86)$$

Integrating Eq. (4.10), we get pressure or energy density of the contribution of valence quarks and antiquarks by using above equation,

$$P_{q\bar{q}}(T, \mu) = \frac{\nu_q}{6\pi^2} \int_0^\infty dp \frac{p^4}{E} [n_q(T, \mu) + n_{\bar{q}}(T, \mu)]. \quad (2.87)$$

Now we can minimize Ω with respect to σ and $\vec{\pi}$ as we mentioned, leading

$$\frac{\partial \Omega}{\partial \sigma} = \lambda^2(\sigma^2 + \vec{\pi}^2 - v^2)\sigma - H + g\rho_s = 0, \quad (2.88)$$

$$\frac{\partial \Omega}{\partial \pi_i} = \lambda^2(\sigma^2 + \vec{\pi}^2 - v^2)\pi_i + g\rho_{ps,i} = 0. \quad (2.89)$$

Here, the scalar and pseudoscalar densities can be expressed as:

$$\rho_s = \langle \bar{q}q \rangle = g\sigma\nu_q \int \frac{d^3\mathbf{p}}{(2\pi)^3} \frac{1}{E} [n_q(T, \mu) + n_{\bar{q}}(T, \mu)], \quad (2.90)$$

$$\vec{\rho}_{ps} = \langle \bar{q}i\gamma_5\vec{\tau}q \rangle = g\vec{\pi}\nu_q \int \frac{d^3\mathbf{p}}{(2\pi)^3} \frac{1}{E} [n_q(T, \mu) + n_{\bar{q}}(T, \mu)]. \quad (2.91)$$

Here we have set the expectation value of the pion field to zero, $\vec{\pi} = 0$, the mass thus become $M^2 = g^2\sigma^2$ in term of energy to calculate the equilibrium quark bath at nonzero T and $\mu = 0$, and at nonzero μ and $T = 0$.

CHAPTER III

MODEL DESCRIPTION

In this Chapter we introduce HIC and freeze-out. Then we have discussed the hydrodynamic evolution. To get the evolution of energy and momentum, we would like to give the information about Einstein tensor. Solving this with the assumption of Bjorken, we will get the Langevin equation which is used to get the evolution of the sigma field. Finally, we test the fluctuation of the field by higher-order cumulants which is the statistical method.

3.1 Heavy-ion collision

When two very high-energy heavy ions collide to each other, the collision creates a very hot and dense medium, a fireball of a fluid-like medium. Then this hot fireball expands and cools down undergoing the phase transition see Figure (3.1).

One distinguishes between two types of freeze-out, the first comes to the chemical freeze-out after which no inelastic collisions occur anymore, resulting in the fixed chemical composition of the system. Then, at the moment when elastic collisions cease as well, one speaks of a thermal or kinetic freeze-out. From the definition, it is clear that the chemical freeze-out will happen before the kinetic freeze-out.

There are properties of the thermal fireball at chemical freeze-out in heavy-ion collisions at all energies. The freeze-out condition is related to the description of the successful particle spectra, it is used for the understanding of particle production. The freeze-out(T, μ) can be obtained by the thermal model describing the ratios of hadron yields produced in nucleus-nucleus collision. The partition function yields the parti-

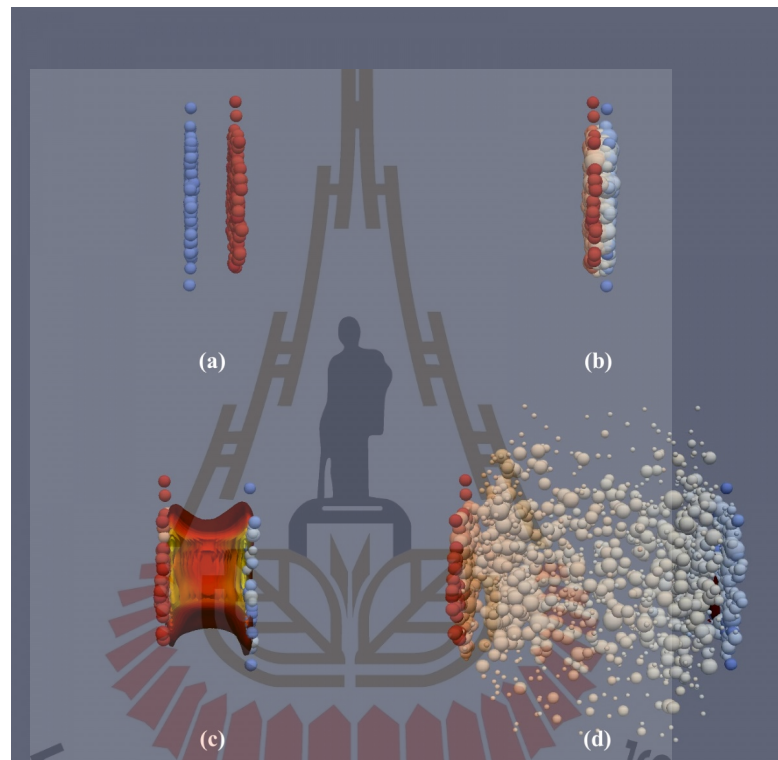


Figure 3.1 (a). Two heavy ion - flattened into a pancake shape since they are traveling near the speed of light - collide into each other. (b). Protons and neutrons dissolve for a brief instant, liberating their constituents (quarks and gluons) to form a Quark-Gluon-Plasma (very hot and dense fireball) (c). The Quark-Gluon-Plasma subsequently decays into thousands of particles (d). Each of these particles provides an information as a foot-print to what occurred inside the collision zone. <https://sciencenode.org/feature/modeling-heavy-ion-collisions-open-science-grid.php>

cle number density n_i for species i and is obtained by the grand canonical ensemble following (Andronic et al., 2006),

$$\ln Z_i = V d_i \int_0^\infty \frac{d^3 p}{(2\pi)^3} \ln[1 \pm \exp(-(E_i - \mu_i)/T)]. \quad (3.1)$$

The above equation gives the particle number density as

$$n_i = N_i/V = -\frac{T}{V} \frac{\partial \ln Z_i}{\partial \mu} = \frac{d_i}{2\pi^2} \int_0^\infty \frac{p^2 dp}{\exp[(E_i - \mu_i)/T] \pm 1}. \quad (3.2)$$

Here, d_i is the spin degeneracy factor. The fermions and bosons are represented by sign +, and -, respectively. In this context, the temperature T_i and chemical potential μ_i are the conjectured values at freeze-out. The chemical potential is given as $\mu_i = \mu_b B_i + \mu_{I_3} I_{3i} + \mu_S S_i + \mu_C C_i$ for baryon number (μ_b), isospin (μ_{I_3}), strangeness (μ_S) and charm (μ_C).

This simple model explains the experimental data from CERN's Super Proton Synchrotron (SPS) up to RHIC measured only elastic collision. The ratios of the particle number is shown in Figure 3.2. To compare with thermal model, we see the effect of baryon is clearly reduced, but temperature is constant at high beam energy. This is corresponding to Bjorken assumption that at sufficiently high energy collisions the mid-rapidity region is approximately net-baryon free.

3.2 Relativistic Hydrodynamics

In this Section, we are discussing hydrodynamics to describe the space-time evolution of the medium created after the collision. In local equilibrium, the condition for hydrodynamics is to have a minimum mean free path less than the size of medium $\lambda \ll L$

For components $\mu = \nu = 0$,

$$\begin{aligned} T_r^{00} &= \frac{\Delta E}{\Delta x \Delta y \Delta z} \\ &= \frac{\Delta E}{\Delta V} \\ &= e. \end{aligned}$$

For components $\mu = \nu \neq 0$,

$$T_r^{\mu\nu} = p.$$

Now energy-momentum tensor $T^{\mu\nu}$ is given by

$$T_{rest} = \begin{pmatrix} e & 0 & 0 & 0 \\ 0 & p & 0 & 0 \\ 0 & 0 & p & 0 \\ 0 & 0 & 0 & p \end{pmatrix}. \quad (3.5)$$

Applying two Lorentz transformations, the energy-momentum tensor in any frame becomes

$$T^{\mu\nu} = \Lambda_\rho^\mu \Lambda_\sigma^\nu T_r^{\rho\sigma} \quad (3.6)$$

$$= \Lambda_0^\mu \Lambda_0^\nu e + \Lambda_i^\mu \Lambda_i^\nu p \quad (3.7)$$

$$= (e + p)u^\mu u^\nu - g^{\mu\nu} p. \quad (3.8)$$

Here, the Minkowski matrix $g^{\mu\nu} = \text{diag}(-1, 1, 1, 1)$ and u^μ is the local four-velocity of the fluid, defined as

$$u^\mu(x) = \gamma(x)(1, \vec{v}(x)), \quad (3.9)$$

where $\gamma = 1/\sqrt{1 - \vec{v}^2}$.

The hydrodynamic equations must conserve energy-momentum and baryon number,

$$\partial_\mu T^{\mu\nu} = 0, \quad (3.10)$$

$$\partial_\mu j_B^\mu = 0. \quad (3.11)$$

Here, the baryon number current $j_B^\mu = n_B(x)u^\mu(x)$ and n_B is the net-baryon density defined in the fluid rest frame (the baryon number is related to the quark number by the factor of 3, i.e. $n_B = n_q/3$). In the rest frame of the fluid, the energy density is a constant of time, $\frac{\partial e}{\partial t} = 0$ and the pressure is constant over space, $\frac{\partial p}{\partial x_i} = 0$. For a moving fluid, we obtain a scalar equation by contracting the conservation of energy with the four-velocity, yielding

$$u^\mu \partial_\mu e + (e + p) \partial_\mu u^\mu = 0. \quad (3.12)$$

3.2.2 Bjorken's scaling solution

After a proper time $\tau_0 \sim 1$ fm, the quarks and gluons are expected to form an equilibrated QGP see Figure 3.3. As soon as the system is in local thermal equilibrium, its evolution can be described by relativistic hydrodynamics (Monnai, 2014), where instead of single particles, energy and baryon densities are propagated according to the corresponding conservation laws. The hydrodynamic stage is especially interesting as it comprises not only the evolution of the QGP but also the subsequent phase transition to the hadronic plasma. At some time τ_f , the hadrons will cease to interact and stream freely into the detector where they are measured. This is called the freeze-out. More precisely, one distinguishes between two types of freeze-out: first comes the chemical freeze-out, after which no inelastic collisions occur anymore, resulting in the fixed

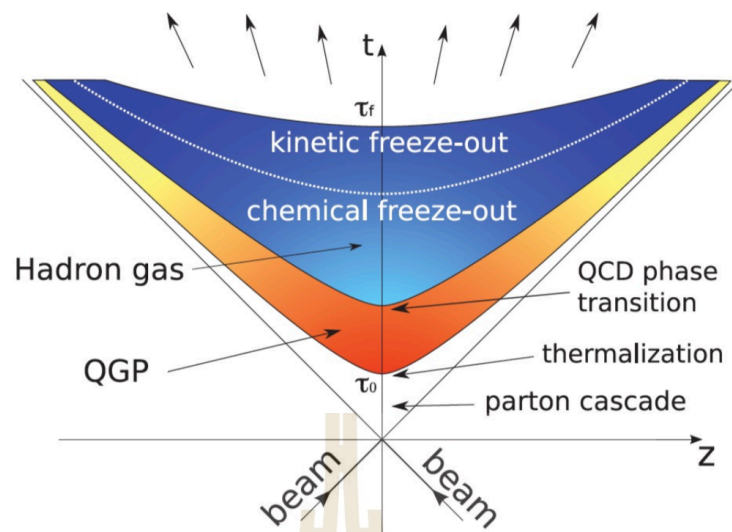


Figure 3.3 The space-time evolution of a heavy-ion collision according to the Bjorken model (Shi et al., 2009).

chemical composition of the system. Then, at the moment when elastic collisions cease as well, one speaks of a thermal or kinetic freeze-out. From the definition, it is clear that the chemical freeze-out will happen before the kinetic freeze-out.

There are two simple pictures of heavy-ion collisions. First, the Landau picture describes the collision process as a complete stop of the nuclei that lost all of their kinetic energy (Landau, 1953). Subsequently, the particles expand hydrodynamically along the beam axis. For higher beam energies in the ultrarelativistic regime, the kinetic energy of the collision can not be deposit anymore due to the large stopping power, and we need to apply the Bjorken picture (Bjorken, 1983) which proposes that the incoming nuclei become transparent by penetrating each other and retaining part of their initial kinetic energy. At mid-rapidity, the net-baryon number is then approximately zero. Due to time dilation, the particles emerge on a hypersurface of constant proper time depicted as a hyperbola in the Minkowski diagram.

For sake of simplicity, we consider a (1+1) dimensional expansion and use the

light cone variables, proper time τ and space-time rapidity y ,

$$\tau = \sqrt{t^2 - z^2}, \quad y = \frac{1}{2} \ln \frac{t+z}{t-z} \quad (3.13)$$

$$t = \tau \cosh y, \quad z = \tau \sinh y. \quad (3.14)$$

All particles are produced in a very short interval around $z = t = 0$ that means longitudinal motion is uniform and transverse motion has vanished. The four-velocity u^μ becomes,

$$u^\mu = \gamma(1, 0, 0, z/t) = (t/\tau, 0, 0, z/\tau) = (\cosh y, 0, 0, \sinh y). \quad (3.15)$$

This is called scaling flow or Bjorken flow. Substituting this into Eq. (3.12), gives us the independence of the pressure on space-time rapidity and, therefore, its boost-invariance:

$$\frac{\partial p(\tau, y)}{\partial y} = 0. \quad (3.16)$$

This means that the pressure is Lorentz invariant. We solve the equation for the time dependent energy density by using the relations $u_\mu \partial^\mu = \frac{\partial}{\partial \tau}$ and $\partial^\mu u_\mu = \frac{1}{\tau}$ in Eq. (3.12) and obtain

$$\frac{\partial e}{\partial \tau} = -\frac{e+p}{\tau}. \quad (3.17)$$

And similarly, the conserved baryon number becomes

$$\frac{\partial n}{\partial \tau} = -\frac{n}{\tau}. \quad (3.18)$$

3.3 Effective model

We will explain how to obtain the mass of the sigma field to determine the correlation length ξ from the linear sigma of the quark-meson model which describes the restoration of chiral symmetry at high T . Previous one, the potential of quark-antiquark contribution reads,

$$\Omega_{qq} = -2N_c N_f T \int \frac{d^3\mathbf{p}}{(2\pi)^3} \left\{ \ln \left[1 + \exp \left(\frac{E - \mu}{T} \right) \right] + \ln \left[1 + \exp \left(\frac{E + \mu}{T} \right) \right] \right\}, \quad (3.19)$$

$$U(\sigma, \vec{\pi}) = \frac{\lambda^2}{4} (\sigma^2 + \vec{\pi}^2 - v^2)^2 - H\sigma. \quad (3.20)$$

Here, $U(\sigma)$ represents the vacuum potential of the σ field corresponding to contribution of thermal quarks. We have the particle energy $E = \sqrt{p^2 + M^2}$, and the effective mass of quarks $M(\sigma) = g\sigma$. The field $q = (u, d)$ has the component of the light quark fields only. The quark-meson coupling g depends on the nucleon mass and is fixed by $g(\sigma) = 940$ MeV in a vacuum.

From this Lagrangian, we get the Langevin equation of motion as (Nahrgang, Leupold, et al., 2011; Herold, Bleicher, et al., 2018; Nahrgang, Herold, et al., 2013)

$$\ddot{\sigma} + \left(\frac{D}{\tau} + \eta \right) \dot{\sigma} + \frac{\delta\Omega}{\delta\sigma} = \xi. \quad (3.21)$$

In the Hubble term $\sim D/\tau$, D is dimension setting $D = 1$, the case of a longitudinal expansion along the direction of the beam axis and the $\dot{\sigma} = d\sigma/d\tau$. Under the assumption of the Bjorken model that the rapidity distribution of the charged particles is boost invariant, we obtain energy and baryon density as

$$de/d\tau = -(e + P)/\tau, \quad dn/d\tau = -n/\tau.$$

The damping coefficient η has been performed as

$$\eta = \frac{12g^2}{\pi} \left[1 - 2n_F \left(\frac{m_\sigma}{2} \right) \right] \frac{1}{m_\sigma^2} \left(\frac{m_\sigma^2}{4} - m_q^2 \right)^{3/2}. \quad (3.22)$$

The damping η and noise $\xi(t, x)$ term in the above equation satisfy the fluctuation-dissipation theorem (Herold, Nahrgang, et al., 2013) :

$$\langle \xi(t)\xi(t') \rangle_\xi = \delta(t - t') \frac{m_\sigma \eta}{V} \coth \left(\frac{m_\sigma}{2T} \right). \quad (3.23)$$

The mass of sigma is characterized by temperature and chemical potential and it is equal to the curvature of the thermodynamic potential in equilibrium,

$$m_\sigma^2 = \left. \frac{\partial^2 \Omega}{\partial \sigma^2} \right|_{\sigma = \langle \sigma \rangle}. \quad (3.24)$$

Similar to what was found in (Nahrgang, Leupold, et al., 2011) and noise ξ is considered Gaussian and white.

CHAPTER IV

RESEARCH METHODOLOGY

In this Chapter, we concentrate on how to calculate the evolution of a fireball by numerical by solving the sigma field equation of motion as shown on flow diagram (4.3). The equation comprises the evolution of the quark field and dissipation-noise in a Bjorken expansion. Next, we investigate higher cumulants of the sigma field equation to locate the critical point. We use a freeze-out to describe σ , N fluctuations as a function of \sqrt{s} .

4.1 Phase transition

The dynamics of the order parameter σ fields and the quark-antiquark fluid will be coupled together. The non-equilibrium equation of motion for the sigma field (N. Cassol-Seewald et al., 2012) is,

$$\partial_\mu \partial^\mu \sigma + \eta \frac{\partial \sigma}{\partial t} + \frac{\delta \Omega_{\bar{q}q}}{\delta \sigma} = \xi(t), \quad (4.1)$$

$$\frac{\partial^2 \sigma}{\partial t^2} + \eta \frac{\partial \sigma}{\partial t} + \frac{\delta \Omega_{\bar{q}q}}{\delta \sigma} = \xi(t), \quad (4.2)$$

Here, the order parameter depended on only time coordinating and η is a damping coefficient as there are a dissipative or the interaction between chiral fields and quarks fluid. $\xi(t)$ represents the stochastic noise as a function of time which is Gaussian and white. The total energy-momentum dissipation from the sigma field is given by

$$\partial_\mu T_q^{\mu\nu} = S^\nu. \quad (4.3)$$

In the absence of the interaction, the source term S^ν vanishes and the energy-momentum of the quarks are conserved. Thus, the total energy-momentum tensor of quarks plus chiral fields is the conserved quantity;

$$\partial_\mu T_q^{\mu\nu} + \partial_\mu T_\sigma^{\mu\nu} = 0 \quad (4.4)$$

$$\partial_\mu T_q^{\mu\nu} = -\partial_\mu T_\sigma^{\mu\nu} = S^\nu. \quad (4.5)$$

Here, the divergence of the energy-momentum tensor for the fields is given by

$$\partial_\mu T_\sigma^{\mu\nu} = -\left(\eta \frac{\partial \sigma}{\partial t} + \frac{\delta \Omega_{\bar{q}q}}{\delta \sigma}\right) \partial^\nu \sigma. \quad (4.6)$$

The derivation of this divergence was shown in (Herold, 2013). The time dependence of the energy density, thus, changes from Eq. (3.17) to

$$\frac{\partial e}{\partial \tau} = -\frac{e+p}{\tau} + \left(\eta \frac{\partial \sigma}{\partial t} + \frac{\delta \Omega}{\delta \sigma}\right) \frac{\partial \sigma}{\partial t}. \quad (4.7)$$

Here,

$$\Omega = -\frac{T}{V} \ln \mathcal{Z} = \Omega_{\bar{q}q} + U(\sigma, \vec{\pi}), \quad (4.8)$$

We will explain how to obtain the chiral phase transition from quark-meson model which describes the restoration of chiral symmetry at high T ,

$$U(\sigma) = \frac{\lambda^2}{4} (\sigma^2 - f_\pi^2)^2 - f_\pi m_\pi^2 \sigma + U_0. \quad (4.9)$$

Here, $U(\sigma)$ represents the vacuum potential of the sigma field corresponding to thermal

quarks potential where the quark and antiquark contribution reads,

$$\Omega_{\bar{q}q} = -2N_c N_f T \int \frac{d^3\mathbf{p}}{(2\pi)^3} \left\{ \ln \left[1 + \exp \left(\frac{E - \mu}{T} \right) \right] + \ln \left[1 + \exp \left(\frac{E + \mu}{T} \right) \right] \right\}. \quad (4.10)$$

To get the phase transition as a function of T, μ we minimize the grand canonical potential,

$$\frac{\partial \Omega(\sigma, T, \mu)}{\partial \sigma} \Big|_{\sigma=\sigma_{eq}} = 0, \quad (4.11)$$

to obtain σ_{eq} . We thus need to find an appropriate condition that the minimize potential occurs setting temperature T_i varying from 0 to 250 MeV and baryochemical potential μ_j varying from 0 to 400 MeV see Figure 4.1. Here all of the solution at equilibrium can express as an array of σ

$$\sigma_{eq}(T_i, \mu_j) = \begin{pmatrix} \sigma_{eq}(T_1, \mu_1) & \sigma_{eq}(T_1, \mu_2) & \cdots & \sigma_{eq}(T_1, \mu_{401}) \\ \sigma_{eq}(T_2, \mu_1) & \sigma_{eq}(T_2, \mu_2) & \cdots & \sigma_{eq}(T_2, \mu_{401}) \\ \sigma_{eq}(T_3, \mu_1) & \sigma_{eq}(T_3, \mu_2) & \cdots & \sigma_{eq}(T_3, \mu_{401}) \\ \vdots & \vdots & \ddots & \vdots \\ \sigma_{eq}(T_{251}, \mu_1) & \sigma_{eq}(T_{251}, \mu_2) & \cdots & \sigma_{eq}(T_{251}, \mu_{401}) \end{pmatrix}. \quad (4.12)$$

In one phase, symmetry is restored, i.e. $\sigma_{eq} \sim 0$), and symmetry is broken at $\sigma_{eq} > 0$.

We can separate the order of phase transition by critical point as second order phase transition. Here we then get our phase transition that they will propagate through the different types of transition (FOPT, CEP, or CO) as shown in Figure 4.2.

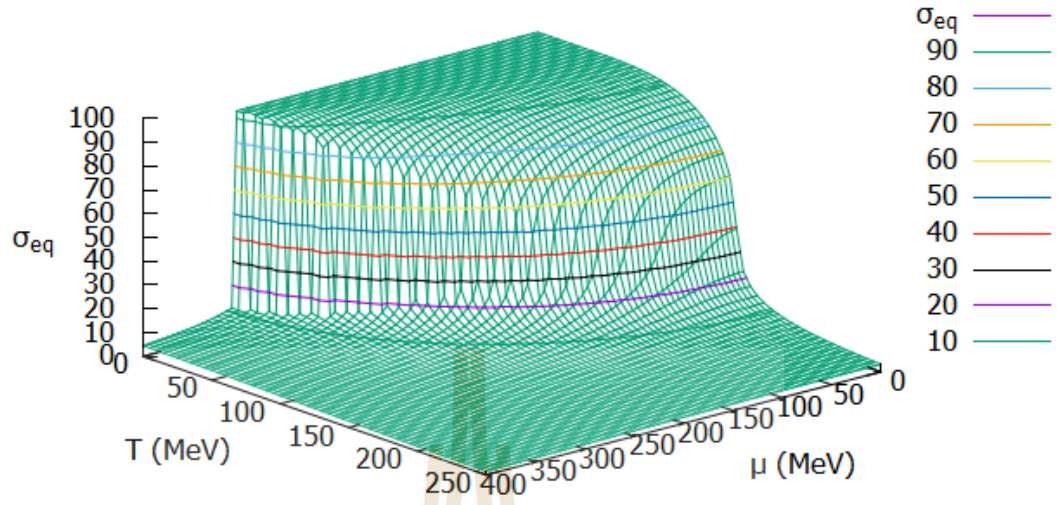


Figure 4.1 The sigma equilibrium at all Temperature T and chemical potential μ space as shown in 3D-plot

4.2 Numerical evolution of sigma field

From the equation of motion for the sigma fields coupled with quark, we have

$$\ddot{\sigma} + \left(\frac{D}{\tau} + \eta \right) \dot{\sigma} + \frac{\delta\Omega}{\delta\sigma} = \xi. \quad (4.13)$$

We use the leap frog algorithm from (N. C. Cassol-Seewald et al., 2007). The iteration of this algorithm by starting with,

$$\frac{\partial\sigma_j}{\partial t} = \dot{\sigma}_j = \frac{1}{2} (\dot{\sigma}_{j+1/2} + \dot{\sigma}_{j-1/2}), \quad (4.14)$$

$$\dot{\sigma}_{j+1/2} = \frac{1}{\Delta t} (\sigma_{j+1} - \sigma_j), \quad (4.15)$$

$$\frac{\partial^2\sigma_j}{\partial t^2} = \ddot{\sigma}_j = \frac{1}{\Delta t} (\dot{\sigma}_{j+1/2} - \dot{\sigma}_{j-1/2}). \quad (4.16)$$

$$(4.17)$$

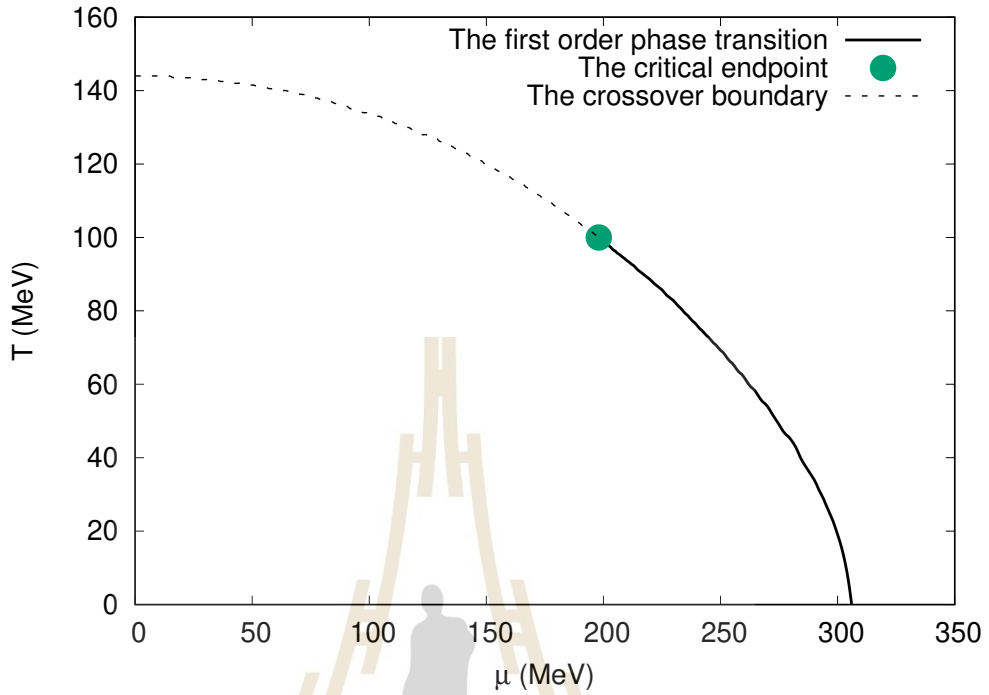


Figure 4.2 The phase structure of chiral phase transition in temperature and quark chemical potential space (T, μ) . It has 3 types of the transition. The chiral first order phase transition ends at $(100, 200)$ MeV. After this critical end point, lies a cross-over region.

Rewriting the Eq. (4.2) in discrete gives,

$$\underbrace{\frac{1}{\Delta t} (\dot{\sigma}_{j+1/2} - \dot{\sigma}_{j-1/2})}_{\frac{\partial^2 \sigma_j}{\partial t^2}} + \underbrace{\eta \frac{1}{2} (\dot{\sigma}_{j+1/2} + \dot{\sigma}_{j-1/2})}_{\eta \frac{\partial \sigma_j}{\partial t}} + \underbrace{\frac{\delta \Omega_{\bar{q}q}(\sigma_j)}{\delta \sigma}}_{\frac{\delta \Omega_{\bar{q}q}(\sigma_j)}{\delta \sigma}} = \xi(j). \quad (4.18)$$

In a compact notation for the iteration, we end up with

$$\dot{\sigma}_{j+1/2} = \frac{1}{(1 + \frac{1}{2}\eta\Delta t)} \left[\dot{\sigma}_{j-1/2} \left(1 - \frac{1}{2}\eta\Delta t \right) \right] - \left[\frac{\delta \Omega_{\bar{q}q}(\sigma_j)}{\delta \sigma} \Delta t + \xi_j \Delta t \right]. \quad (4.19)$$

We then update σ by

$$\sigma_{j+1} = \sigma_j + \dot{\sigma}_{j+1/2} \Delta t. \quad (4.20)$$

Consider the noise term $\xi(t)$, we have the fluctuation-dissipation relation,

$$\langle \xi(t) \xi(t') \rangle_\xi = \delta(t - t') \frac{m_\sigma \eta}{V} \coth \left(\frac{m_\sigma}{2T} \right). \quad (4.21)$$

On our calculation, we get damping η and correlation length $\langle \xi(t) \xi(t') \rangle_\xi$ by equilibrium in vacuum from star. For $t = t'$, Gauss distribution and small m_σ compared with QCD regime give an amplitude

$$\langle \xi(t)^2 \rangle = \frac{2\eta T}{V \Delta t}. \quad (4.22)$$

the random fluctuation can then be written as

$$\xi_i = \sqrt{\frac{2\eta_i T}{V \Delta t}} G_i, \quad (4.23)$$

where $G_{i,n}$ is obtained from a zero-mean Gaussian distribution. Here, index $i = 1, 2$ label the Gaussian noises and white noises, respectively. We use Marsaglia polar method. For this, we consider random variables W_1, W_2 which are uniformly distributed on $[-1, 1]$ such that $W_1^2 + W_2^2 < 1$. It can be generated as follows.

$$W_1 = 2U_1 - 1 \quad W_2 = 2U_2 - 1, \quad (4.24)$$

where $0 \leq W_1^2 + W_2^2 < 1$. Therefore, X is generated by

$$X = \sqrt{-2 \ln(W_1^2 + W_2^2)} \frac{W_1}{\sqrt{W_1^2 + W_2^2}}. \quad (4.25)$$

Gaussian random variable reads

$$G = X * \sigma + \mu \quad . \quad (4.26)$$

From equation (4.23), we consider a zero-mean Gaussian

$$\xi_{i,n} = \sqrt{\frac{2\eta_i T}{V\Delta t}} X_{i,n} , \quad (4.27)$$

where U_1, U_2 are random variable.

4.3 Numerics of hydrodynamic evolution

We have the energy in form of non-linear differential equation as a function as shown in Eq. (4.7),

$$\frac{\partial e}{\partial \tau} = \frac{e + p}{\tau} + \left(\frac{\partial \Omega}{\partial \sigma} + \eta \frac{\partial \sigma}{\partial \tau} \right) \frac{\partial \sigma}{\partial \tau}, \quad (4.28)$$

$$f(e, \tau) = \frac{e + p}{\tau} + \left(\frac{\partial \Omega(\sigma, T, \mu)}{\partial \sigma} + \eta \frac{\partial \sigma(T, \mu)}{\partial \tau} \right) \frac{\partial \sigma(T, \mu)}{\partial \tau}. \quad (4.29)$$

The derivative of equation is obtained by a forth order adaptive Rung-Kutta algorithm,

$$\frac{dy}{dt} = f(y, t) \quad (4.30)$$

$$k_1 = f(x_j, t_j) \quad (4.31)$$

$$k_2 = f\left(x_j + \frac{h}{2}k_1, t_j + \frac{h}{2}\right) \quad (4.32)$$

$$k_3 = f\left(x_j + \frac{h}{2}k_2, t_j + \frac{h}{2}\right) \quad (4.33)$$

$$k_4 = f(x_j + hk_3, t_j + h) \quad (4.34)$$

$$y_{j+1} = y_j + \frac{h}{6}(k_1 + 2k_2 + 2k_3 + k_4). \quad (4.35)$$

Here, h is a step size (time-step $\Delta\tau$). We choose the time-step $\Delta\tau$ equal to 0.08 fm,

$$k_1 = f(e_j, \tau_j) \quad (4.36)$$

$$k_2 = f\left(e_j + \frac{d\tau}{2}k_1, \tau_j + \frac{d\tau}{2}\right) \quad (4.37)$$

$$k_3 = f\left(e_j + \frac{d\tau}{2}k_2, \tau_j + \frac{d\tau}{2}\right) \quad (4.38)$$

$$k_4 = f(e_j + d\tau k_3, \tau_j + dt), \quad (4.39)$$

$$e_{j+1} = e_j + \frac{d\tau}{6}(k_1 + 2k_2 + 2k_3 + k_4). \quad (4.40)$$

Similarly, the quark density n as a function of time reads

$$\frac{\partial n}{\partial \tau} = -\frac{n}{\tau}. \quad (4.41)$$

Here, we have $f(n, \tau) = -n(\sigma_j, T_j, \mu_j)/\tau$

$$k_1 = f(n_j, \tau_j) \quad (4.42)$$

$$k_2 = f(n_j + \frac{d\tau}{2}k_1, \tau_j + \frac{d\tau}{2}) \quad (4.43)$$

$$k_3 = f(n_j + \frac{d\tau}{2}k_2, \tau_j + \frac{d\tau}{2}) \quad (4.44)$$

$$k_4 = f(n_j + d\tau k_3, \tau_j + dt), \quad (4.45)$$

$$n_{j+1} = n_j + \frac{d\tau}{6}(k_1 + 2k_2 + 2k_3 + k_4). \quad (4.46)$$

The pressure at each time step is calculated from,

$$p_{j+1} = -\Omega_{q\bar{q}}(\sigma_{j+1}, T_{j+1}, \mu_{j+1}). \quad (4.47)$$

Here, T_{j+1} and μ_{j+1} are updated in advance. The updated energy density e_{j+1} and quark density n_{j+1} are put used for solving the temperature T_{j+1} and quark chemical potential μ_{j+1} according to the thermodynamics relation Eq. (2.3.4).

4.4 Central moment and Cumulants

In statistics, we characterize distribution by moments/cumulants. Experimentally, we measure net-proton number (proton number minus antiproton number), $N_{p-\bar{p}} = N_p - N_{\bar{p}}$. We use N to represent the net-proton number $N_{p-\bar{p}}$ in one event. The average value over the total event is defined as $\mu = \langle N \rangle$, where $\langle N \rangle$ is the average for one event. The deviation of N from the mean value can be written as

$$\delta N = N - \langle N \rangle. \quad (4.48)$$

With the evolution of the sigma field, we probe event-by-event fluctuation of the field at each time step τ_i . We can define cumulants of various order of event-by-event

$$C_1 = \langle \sigma \rangle, \quad (4.49)$$

$$C_2 = \langle (\delta\sigma)^2 \rangle, \quad (4.50)$$

$$C_3 = \langle (\delta\sigma)^3 \rangle, \quad (4.51)$$

$$C_4 = \langle (\delta\sigma)^4 \rangle - 3\langle (\delta\sigma)^2 \rangle^2. \quad (4.52)$$

We can get the event averaged sigma field by,

$$\langle \sigma(t) \rangle = \frac{1}{N_{event}} \sum_i \sigma(i, t). \quad (4.53)$$

To get the second-order cumulant, we have to calculate the average of square of sigma,

$$\langle \delta\sigma^2 \rangle = \langle \sigma^2 \rangle - \langle \sigma \rangle^2. \quad (4.54)$$

Now, we have the first moment as the mean, the second moment as the variance measured how much the probability distribution is spread from the mean, The third moment as skewness that measures the symmetry of distributions and the fourth moment as kurtosis which is the measurement of tailedness of distributions. These higher order moments can be written in form of cumulant ratios as

$$M = C_1, \quad (4.55)$$

$$\sigma^2 = C_2, \quad (4.56)$$

$$S = \frac{C_3}{(C_2)^{3/2}}, \quad (4.57)$$

$$\kappa = \frac{C_4}{(C_2)^2}. \quad (4.58)$$

The chiral phase transition can be disclosed by event-by-event fluctuations of conserved quantities such as the net-proton, net-baryon, and net-charge given by

$$N_p = N_{proton} - N_{antiproton}, \quad (4.59)$$

$$N_B = N_{baryon} - N_{antibaryon}, \quad (4.60)$$

$$N_{Ch} = N_{Ch^+} - N_{Ch^-}. \quad (4.61)$$

We can represent these quantities by N then apply the grand canonical ensemble to find the expectation values of these quantities given by

$$\langle N \rangle = \frac{1}{Z} \sum N e^{-\frac{(E-\mu N)}{T}} = T \frac{\partial(\ln Z)}{\partial \mu}. \quad (4.62)$$

We have used that $P = (T/V)\ln Z$ then the average values are given by

$$\langle N \rangle = V \frac{\partial P}{\partial \mu}. \quad (4.63)$$

Now we can write the fluctuation of these quantities in form of its pressure respective to chemical potential μ such as

$$\langle \delta N^2 \rangle = \langle N^2 \rangle - \langle N \rangle^2, \quad (4.64)$$

$$= T \frac{\partial \langle N \rangle}{\partial \mu}, \quad (4.65)$$

$$= TV \frac{\partial^2 P}{\partial \mu^2}. \quad (4.66)$$

The cumulants are related to the susceptibilities of the system which is the derivative of the pressure with respect to the chemical potential. The generalized susceptibilities are given by

$$\chi_n = \frac{\partial^n (p/T^4)}{\partial (\mu/T)^n}, \quad (4.67)$$

It is now easy to write the susceptibilities in the form of high order moments,

$$\begin{aligned}
 \chi_1 &= \frac{1}{VT^3} \langle N \rangle = M, \\
 \chi_2 &= \frac{1}{VT^3} \langle \delta N^2 \rangle = \sigma^2, \\
 \chi_3 &= \frac{1}{VT^3} \langle \delta N^3 \rangle = S\sigma^3, \\
 \chi_4 &= \frac{1}{VT^3} \left[\langle \delta N^4 \rangle - 3\langle \delta N^2 \rangle^2 \right] \\
 &= \kappa\sigma^4.
 \end{aligned}$$

Experimentally, the dependence on volume and temperature of these fluctuations is hard to measure directly. We therefore focus on ratios of cumulants to get rid of effect of T and V ,

$$\frac{\chi_2}{\chi_1} = \frac{\langle \delta N^2 \rangle}{\langle N \rangle} = \frac{\sigma^2}{M}, \quad (4.68)$$

$$\frac{\chi_3}{\chi_2} = \frac{\langle \delta N^3 \rangle}{\langle \delta N^2 \rangle} = S\sigma, \quad (4.69)$$

$$\frac{\chi_4}{\chi_2} = \frac{\langle \delta N^4 \rangle}{\langle \delta N^2 \rangle} - 3\langle \delta N^2 \rangle = \kappa\sigma^2. \quad (4.70)$$

The above cumulants have been measured by experiment, but in our model, we determine the sigma field instead of the number particle. The field σ is not a conserved quantity, but we can connect the fluctuations of the order parameter field σ to the fluctuations of the observable quantities by effective field. The fluctuations of the order parameter field $\sigma(x)$ near a critical point can be described by the probability distributions as:

$$P[\sigma] \sim \exp\{-\Omega[\sigma(x)]/T\} \quad (4.71)$$

where Ω is the effective action functional for the field σ and can be expanded in powers

of σ ,

$$\Omega = \int d^3x \left[\frac{(\nabla\sigma)^2}{2} + \frac{m_\sigma^2}{2}\sigma^2 + \frac{\lambda_3}{3}\sigma^3 + \frac{\lambda_4}{4}\sigma^4 + \dots \right]. \quad (4.72)$$

Consider the infinitesimal change of the field $\delta\sigma$, leads to a change of the effective mass of the particle by the amount $\delta m = g\delta\sigma$. We have the fluctuations δf_k of the momentum space distribution function f_k of the coupling net protons in sigma model defined as

$$\delta f_k = \delta f_k^0 + \frac{\partial n_p}{\partial m} g \delta\sigma. \quad (4.73)$$

The first term δf_k^0 is the purely statistical fluctuations, and the second is the distribution n_p for a particle of a given mass around the equilibrium. We have the fluctuation of the multiplicity $N = V d \int_f \square$ given by

$$\delta N = \delta N^0 + V g \delta\sigma d \int_k \frac{\partial n_p}{\partial m}, \quad (4.74)$$

where d is the degeneracy factor of proton. Term δN^0 can be approximated by a Poisson statistics under assuming $n_p \ll 1$, we can use the expectation of net-proton number for this term. Now we can express the corresponding moments in terms of the σ fluctuations. For example, the 4-th moment can be expressed to leading order as

$$\langle (\delta N)^4 \rangle_c = \langle N \rangle + \langle \sigma_V^4 \rangle_c \left(\frac{g d}{T} \int_k \frac{n_p}{\gamma_k} \right)^4 + \dots, \quad (4.75)$$

where $\gamma_k = (dE_p/dm)^{-1}$ is the relativistic gamma-factor of a particle with momentum k and mass m . The first term is the Poisson baseline. By this, we can calculate N-cumulants from σ -cumulants. We change integral on 4 momenta k by

$$\int_{\mathbf{k}} \equiv \int \frac{d^3\mathbf{k}}{(2\pi)^3}. \quad (4.76)$$

Now the fluctuation of the proton that is easy to integrate by numerical obtain

$$\delta N = \delta N^0 - \langle \sigma_V \rangle \left(\frac{g m_p d}{2T\pi^2} \int_0^\infty \frac{dk k^2 n_p}{E} \right). \quad (4.77)$$

We can get an expression for higher-order fluctuations by assuming $\langle \delta \sigma \delta N \rangle = 0$, i.e. the 4-th cumulant can be expressed as

$$\langle (\delta N)^4 \rangle_c = \langle N \rangle + \langle \sigma_V^4 \rangle_c \left(\frac{g m_p d}{2T\pi^2} \int_0^\infty \frac{dk k^2 n_p}{E} \right)^4, \quad (4.78)$$

where $n_p = 1.0 / (\exp((E - \mu_B)/T) + 1)$. We can integrate numerically using Simpson's rule. An elementary computation reveals that

$$\int_a^b f(k) dk = \frac{b-a}{6} (f(a) + 4f(c) + f(b)). \quad (4.79)$$

Here, $f(k) = k^2 n_p / E$. a is lower limit and b is upper limit with $b = a + h$, h labelled step size, c is equal to $(a+b)/2$.

4.4.1 Statistical Error

The statistical error for for cumulants ratios is estimated from the delta theorem (Luo, 2012) for normal distributions. The error of the cumulant ratios is proportional to the standard deviation of distribution as

$$error\left(\frac{C_r}{C_2}\right) \propto \frac{\sigma^{r-2}}{\sqrt{n}}, \quad (4.80)$$

where r^{th} is the order of cumulants,
 n is the number of events,
 C_2 is the variance (σ^2).

The error of skewness and kurtosis is given by the following formula

$$error(S\sigma) = \sqrt{6} \frac{\sigma}{\sqrt{n}}, \quad (4.81)$$

$$error(\kappa\sigma^2) = \sqrt{24} \frac{\sigma^2}{\sqrt{n}}. \quad (4.82)$$

4.5 Relation of initial condition to beam energy

Table (4.1) are summarized the thermal model fit with the collision beam energy. To extend the descriptions over a wide range of beam energies, we see the beam energy is increasing with the freeze-out temperature T and reducing with the baryon chemical potential μ_B . Our analysis depends on the most recent results obtained in statistical-thermal model fits Au+Au and Pb+Pb systems. Thermal model results gives the first a polynomial fit,

$$T(\mu_B) = a - b\mu_B^2 - c\mu_B^4. \quad (4.83)$$

Here, $a = 0.166 \pm 0.002$ GeV, $b = 0.139 \pm 0.016$ GeV⁻¹ and $c = 0.053 \pm 0.021$ GeV⁻³.

The energy dependence of the baryon chemical potential can be parameterized as:

$$\mu_B(\sqrt{s}) = \frac{d}{1 + e\sqrt{s}}, \quad (4.84)$$

with $d = 1.308 \pm 0.028$ GeV and $e = 0.273 \pm 0.008$ GeV⁻¹ (Cleymans et al., 2006).

4.6 Flow diagram

4.6.1 Get the susceptibility of the system computed in theoretical calculations

Firstly, we import the files that give the calculation from star as a function of (T, μ) consist of `temperatureSigma(100651)`, `temperatureEtasigma(100651)`, `temperaturePress(100651)`, `temperaturesigmaPress(100651)`

4.6.2 Initialize Hydro and Fields

Then the initial condition (T_0, μ_0) are chosen such that they will propagate through the difference types of transition (FOPT, CEP or CO). We also apply the dimpling η and White/Gaussian noise (ξ) in vacuum

4.6.3 Evolve Fluid-dynamics

We solve the equation of motion (Langevin equation) on numerical method by using leap frog algorithm then the equation give eq. (4.18). This equation consist of hydrodynamic equation energy and quark density (e, n) see in Section 4.3.

4.6.4 Cumulants

On this part, we update the sigma field as a function of time event by event fluctuation and then update (T, μ) . Now we obtain the sigma field event by event fluctuation. To calculate cumulant, we need the sigma field average then using eq. (4.68-4.70). We stop iteration when all of cumulant are converge as the same value.

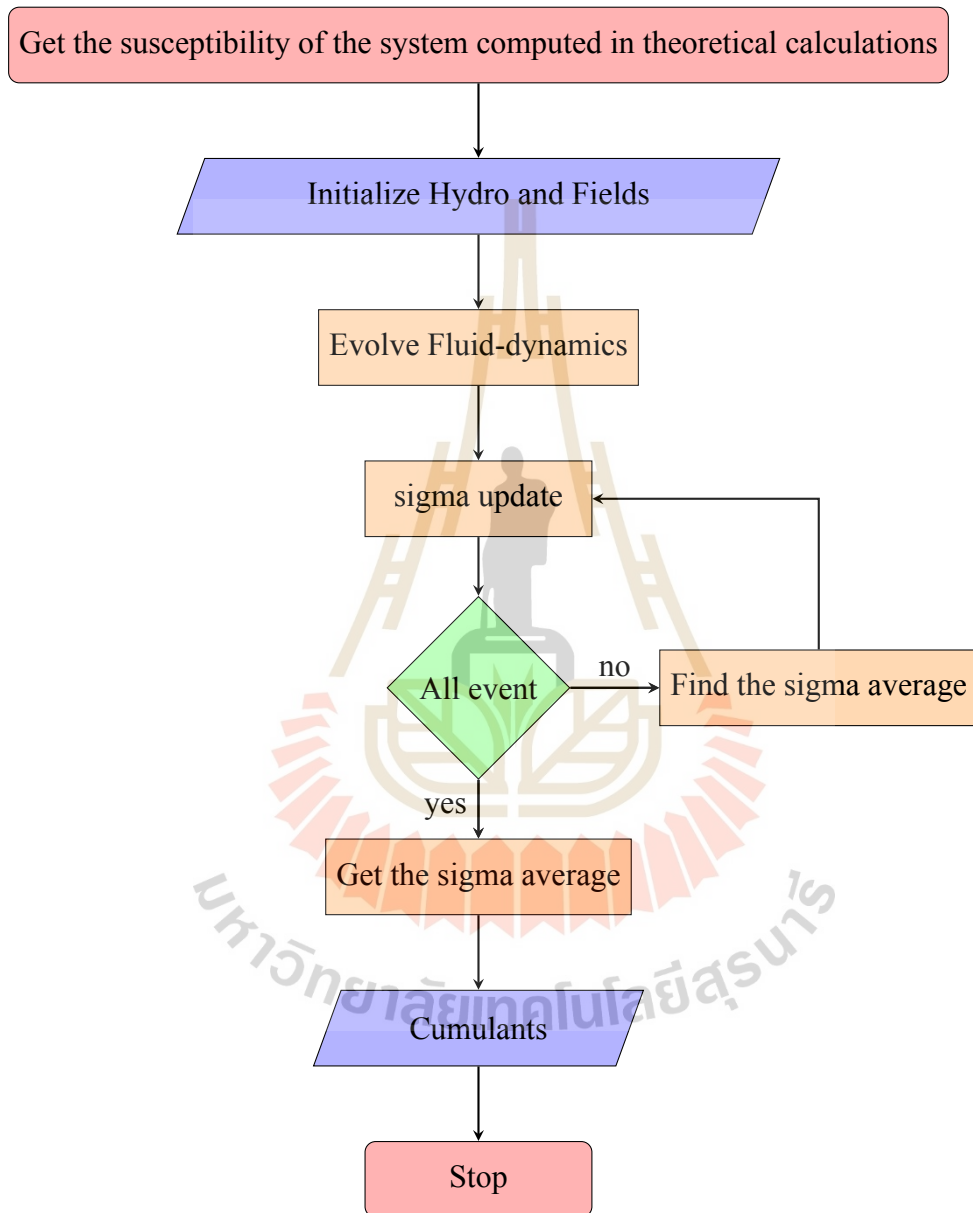


Figure 4.3 We solve the evolution of a fireball by simulation as shown in the flow diagram calculating cumulants of σ .

Table 4.1 Results obtained in statistical-thermal model fits to Au+Au and Pb+Pb collision systems by numerous groups over a wide range of energies. The checked entries have been included in the fits to determine the $T(\mu_B)$ and $\mu_B(\sqrt{s})$.

Collision System and Energy	T (MeV)	μ_B (MeV)	Include in Fits
RHIC			
Au+Au $\sqrt{s} = 200$ AGeV	177 ± 7	29 ± 6	
	163 ± 4	24 ± 4	
	165.6 ± 4.5	28.5 ± 3.7	
Au+Au $\sqrt{s} = 130$ AGeV	169 ± 6	38.1 ± 4.2	✓
	174 ± 7	46 ± 5	✓
	165 ± 7	41 ± 5	✓
SPS			
Pb+Pb 158 AGeV $\sqrt{s} = 17.3$ AGeV	157.5 ± 2.2	248.9 ± 8.2	✓
	154.6 ± 2.7	245.9 ± 10.0	✓
	161.0 ± 6.0	260.0 ± 30	✓
Pb+Pb 80 AGeV $\sqrt{s} = 12.3$ AGeV	153.5 ± 4.1	298.2 ± 9.6	✓
	149.9 ± 5.1	293.8 ± 11.0	✓
	155.0 ± 5.0	284.0 ± 15.0	✓
Pb+Pb 40 AGeV $\sqrt{s} = 8.77$ AGeV	146.1 ± 3.0	382.4 ± 9.1	✓
	143.0 ± 3.1	380.8 ± 8.9	✓
	148.0 ± 5.0	367.0 ± 14.0	✓
Pb+Pb 30 AGeV $\sqrt{s} = 7.62$ AGeV	140.1 ± 3.3	413.7 ± 16.3	✓
	144.3 ± 4.7	406.0 ± 19.1	✓
Pb+Pb 20 AGeV $\sqrt{s} = 6.27$ AGeV	131.3 ± 4.5	466.7 ± 12.9	✓
	135.8 ± 5.2	472.5 ± 13.7	✓
AGS			
Au+Au 11.6 AGeV $\sqrt{s} = 4.86$ AGeV	18.7 ± 3.1	554.4 ± 13.0	✓
	119.2 ± 5.3	578.8 ± 15.4	✓
	123.0 ± 5.0	558.0 ± 15.0	✓
SIS			
Au+Au 1.0 AGeV $\sqrt{s} = 2.32$ AGeV	52 ± 1.5	822	✓
	49.6 ± 1	810 ± 15	✓
	49.7 ± 1.1	818 ± 15	✓
	58 ± 4	792 ± 7	✓
Au+Au 0.8 AGeV $\sqrt{s} = 2.24$ AGeV	54 ± 2	808 ± 5	✓

CHAPTER V

RESULTS AND DISCUSSIONS

From the previous Chapter, we have the program that is used to solve the evolution of the sigma field and its fluctuation by using the Bjorken model coupled to the Langevin equation. This chapter we will conclude all of the result form the numerical. Firstly we would like to show the trajectory of fireball with different initial condition evolving on chiral phase transition and freeze-out. Then we find the proper event to get the higher cumulants on the sigma field. Finally we obtain the net-baryon number fluctuation to compare with the experimental.

5.1 Chiral Phase transition

From the previous Chapter, we have the grand canonical potential $\Omega(\sigma)$ of the chiral model. The minimizing of the potential at a ground state $\left. \frac{\partial \Omega}{\partial \sigma} \right|_{\sigma=\sigma_{eq}}$ gives to be zero. We have the symmetry restored phase, the $\sigma_{eq} \sim 0$ and the symmetry breaking phase, the $\sigma_{eq} > 0$. Consider the non-vanished σ_{eq} , This case is occur in range of $T < T_c$. To separate the first order phase transition and the crossover, the critical point is required. We get the phase boundary by the highest derivative of the σ to the Temperature i.e. $\frac{\partial \sigma(T, \mu)}{\partial T}$. If we consider the grand canonical potential, it would be flat at the critical point. That mean the second derivative of the potential should be zero. Although, it has no latent heat. The critical point has a divergence of susceptibility and correlation length eq. (4.67). This divergence evokes a variety of phenomena that might serve as an experimental signal for locating a critical point. Here, we get the critical point at $(T_c, \mu_c) = (100, 200)$ MeV. Now it is easy to find the first order for $T < T_c$, the σ_{eq} is

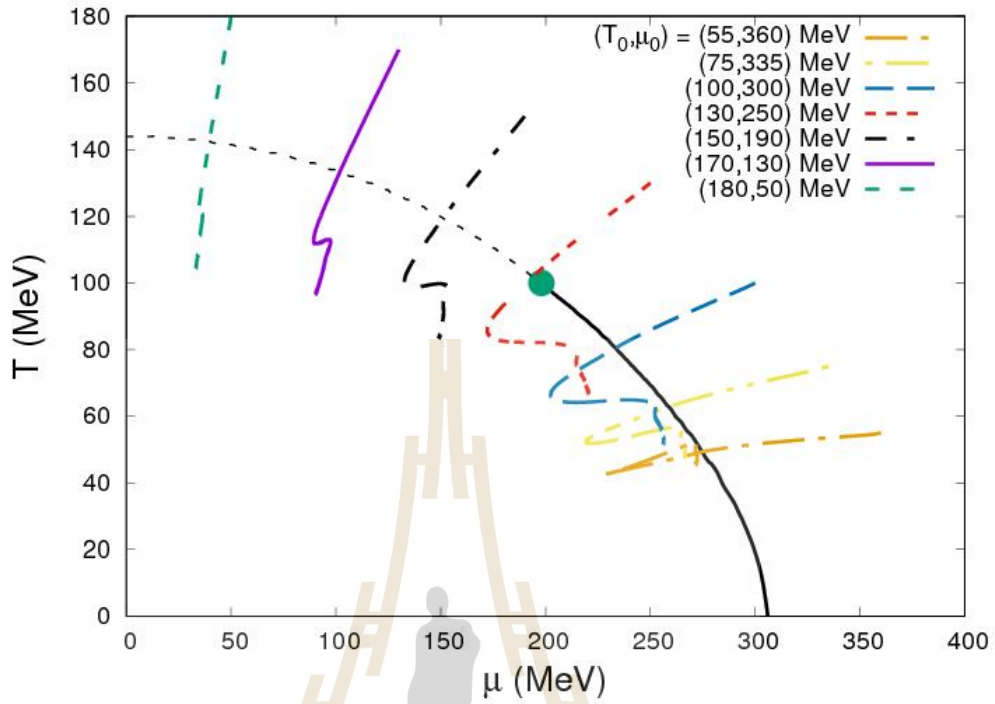


Figure 5.1 The phase structure of chiral phase transition in different initial conditions (T_{int}, μ_{int}) alongside trajectory of fireball.

approximate to be 0. As shown in the figure 5.1, The solid line represent the first order phase transition and the critical point labelled green point. The evolution of the sigma field is obtained by Langevin equation extract (T, μ) from eq. (4.13). We input different initial conditions (T_{int}, μ_{int}) . The sigma field evolve on equation from hydrodynamic equilibrium as

$$n(\sigma, T, \mu) = \frac{\partial p(\sigma, T, \mu)}{\partial \mu} \quad (5.1)$$

$$e(\sigma, T, \mu) = T \left(\frac{\partial p(\sigma, T, \mu)}{\partial T} \right) - p(\sigma, T, \mu) + \mu n(\sigma, T, \mu). \quad (5.2)$$

By above equation, we then get T, μ from comparing the energy to our simulation. It should get the approximate same value. Then the Figure 5.1 show the evolved fireball

on the chiral phase transition. The phase diagram shows the temperature as a function of quark chemical potential. At a small chemical potential, we called the crossover region and the endpoint labelled critical point or second order phase transition. The rest of the boundary is represented by the first order phase transition. The trajectory is referred to as the evolution of (T, μ) as a function of time on the phase transition.

5.2 Freeze-out condition

As mentioned on the previous Chapter, we require energy dependence of the chemical freeze-out parameters T and μ_B measured the quark gluon plasma transit to the hadronic medium at the equilibrium sigma field and detectable on a detector. The freeze-out will help us compare to the experiment. We obtain the relation function of beam energy and baryochemical potential μ_B and temperature T as shown in Figure 5.2. From equation (4.84), we input the 9 beam energy \sqrt{s} corresponding to Table (4.1). We then extract (T, μ) by eq. (4.83). We obviously see the temperature is increasing, while the baryon chemical potential is decreasing as a function of beam energy see in Figure 5.2. Then we connect directly the freeze-out curve on the chiral phase transition by scaling factor to the crossover region. At zero baryochemical potential $\mu_B \sim 0$, we can get the temperature from eq.(4.83) at the freeze-out. We will see curve that it is not corresponding with the chiral phase transition. To corrected the baryochemical potential, we need the scaling factor to multiply with the freeze-out curve to fit it to chiral phase transition. The scaling factor is required $T_{freeze-out}/T_{chiral}$. From eq. (4.83) at small baryochemical potential $\mu_B = 0$, we have $T_{freeze-out}(\mu_m = 0) = 166$ MeV but the chiral obtain the $T_{chiral}(\mu_m = 0) \sim 145$. The freeze-out curves have been obtained by dotted line fit to chiral phase transition see Figure 5.3.

From the freeze-out of (T, μ) , we obtain chemical freeze-out on chiral phase transition is related to the particle production. Moreover we see the trajectories passing

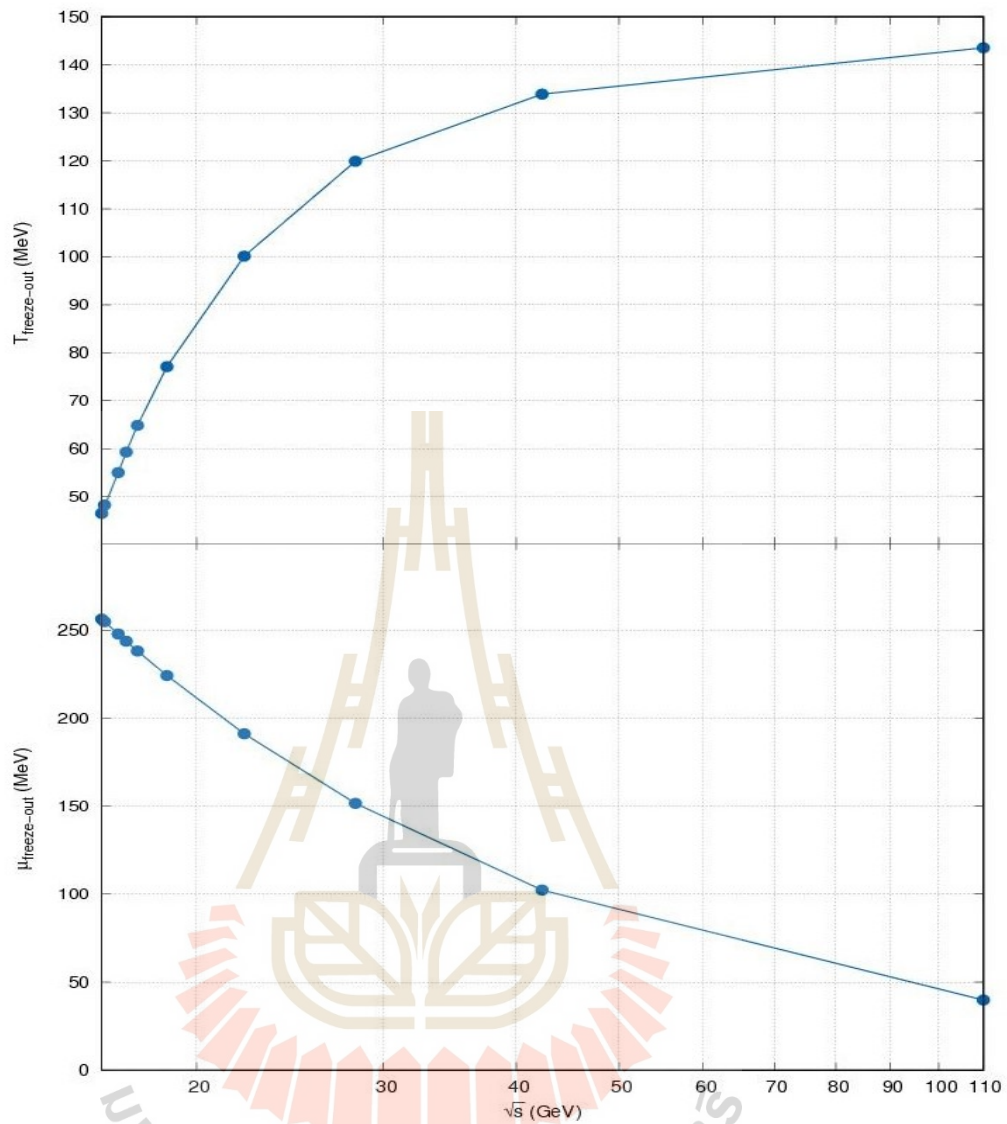


Figure 5.2 The energy dependence of temperature T and quark chemical potential μ_q .

through the first-order phase transition cross the freeze-out curve twice. For these cases, we calculate the cumulants at both crossing points to give a range of possible values.

5.3 The number of event

In this Section, we obtain the sufficient number of events to test fluctuations of higher order cumulants. We input the number events form 10,000 to 100,000 events to test the higher order cumulant appearance as a function of initial condition of bary-

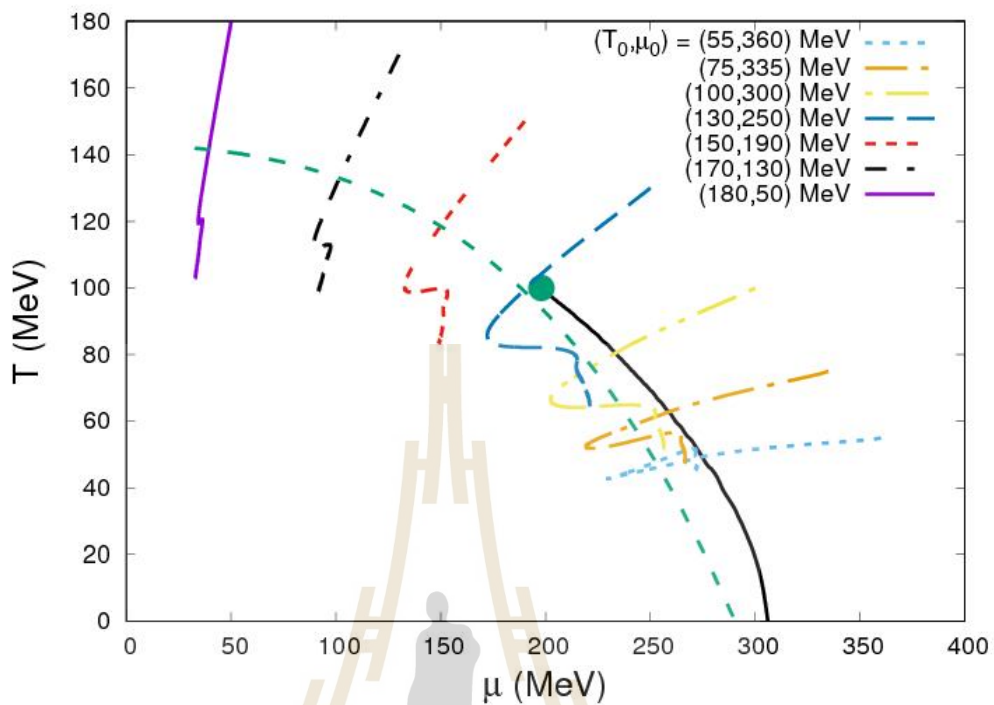


Figure 5.3 The phase structure of chiral phase transition for freeze-out condition is labelled dotted-line.

ochemical potential. We see all of fluctuation get closer to each other depends on a increasing number of events as shown on Figure 5.4. Now we choose 100,000 events which is the maximum that we can do it to solve the higher fluctuation with different beam energy in the next section.

5.4 Fluctuation of sigma field

We initialize the field and fluid in equilibrium at several starting points in the chirally restored phase, see the beginning of the trajectories in the phase diagram of the quark-meson model, Figure 5.1. These points are conveniently characterized by a choice of initial values (T_0, μ_0) . The coupled system of field and fluid is then evolved according to eqs. (4.13) and (4.7) which gives an evolution of T and μ that can be seen

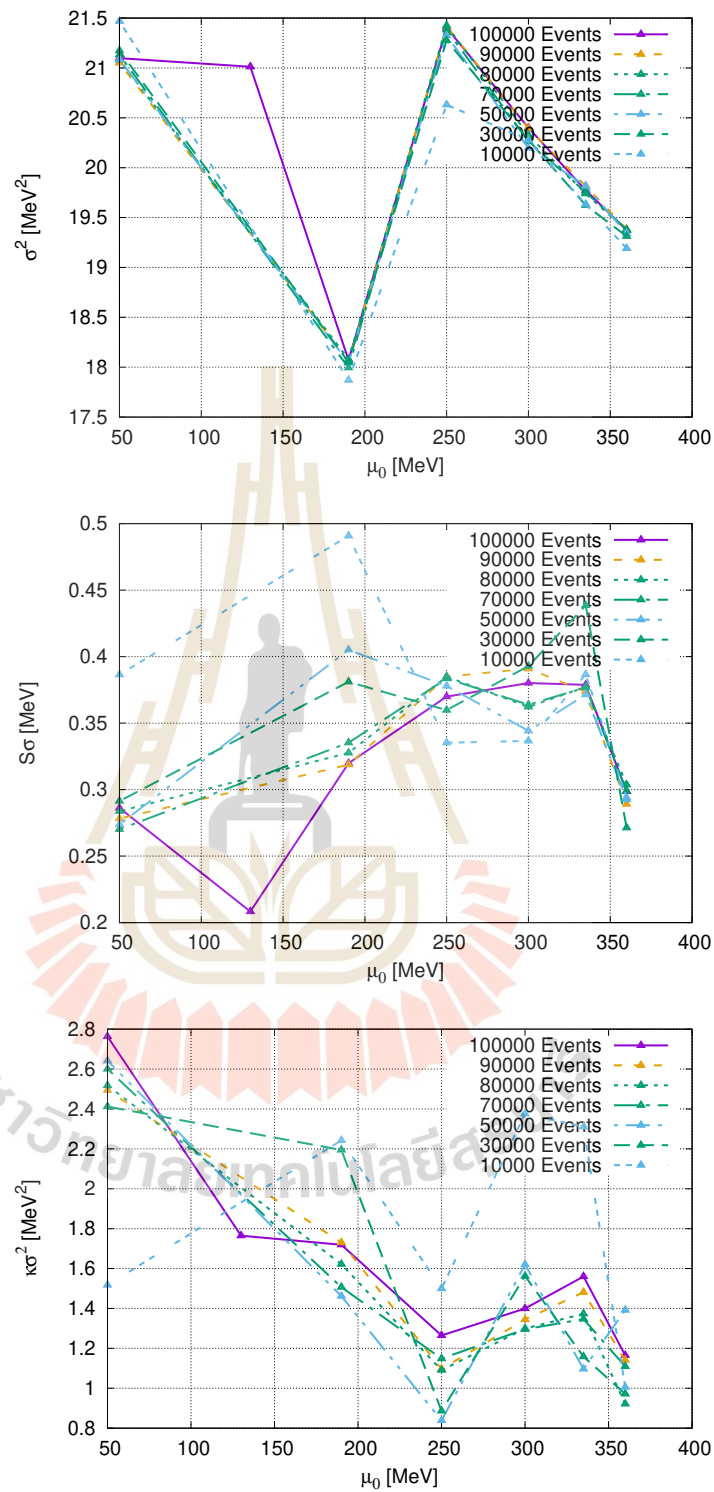


Figure 5.4 σ^2 , $S\sigma$ and $\kappa\sigma^2$ as a function of initial condition of baryochemical potential μ_B . The different colored labelled as the different number of event.

in the same figure.

The point where the trajectories hit the dashed freeze-out line is used to determine the event-by-event fluctuations. We hereby use a number of $N = 10^5$ events which are randomized through the stochastic noise term ξ that yields a non-deterministic evolution. The bending of the trajectories has been discussed in previous publications (Herold, Kittiratpattana, et al., 2019). It is particularly worth noting here that, as a consequence of this behavior, the trajectories passing through the first-order phase transition cross the freeze-out curve twice. For these cases, we calculate the cumulants at both crossing points to give a range of possible values.

This section presents the energy dependence for the cumulants of sigma fields as the order parameter. We investigated the second order of cumulant as the variance σ^2 , the third order of cumulant as the skewness $S\sigma$ and the fourth order of cumulant as the kurtosis $\kappa\sigma^2$ with different initial condition (T, μ) , respectively.

Figure 5.5 shows the so obtained σ^2 , $S\sigma$ and $\kappa\sigma^2$ versus beam energy \sqrt{s} . We note that for all these cases, the consideration of the spinodal region and double-crossing of the freeze-out curve leads to an increased range of possible cumulant values for the lowest beam energies. The variance, which is more or less constant, decreases by a factor of 2 after passing through the second crossing. A similar effect is observed for the skewness, though somewhat less dramatic. The most dramatic impact is seen in the kurtosis. Although it increases monotonically within error bars, we see a clear sign change at beam energy $\sqrt{s} \sim 3$ GeV. As argued in (M. A. Stephanov, 2011) strong negative values of the kurtosis of the order parameter are understood as a direct consequence of a first-order phase transition.

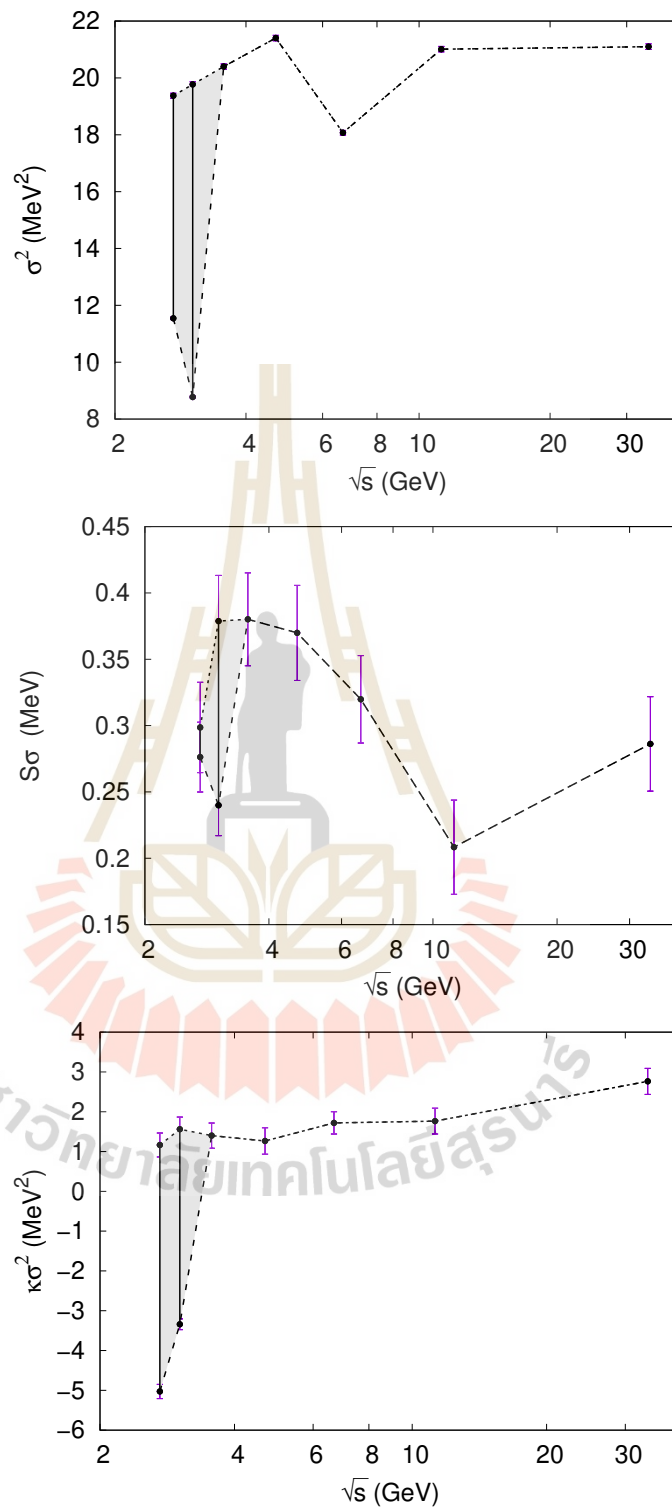


Figure 5.5 σ^2 (a) , $S\sigma$ (b) and $\kappa\sigma^2$ (c) of the sigma field as a function of beam energy \sqrt{s} .

5.5 Fluctuation of the net-baryon number

As introduced previously, we propose the fluctuation net-proton proxy to the fluctuation of the sigma field by using perturbation of effective mass. This quantity can obtain from the experiment. The high order moment of net-proton is related to the susceptibility.

The Figure 5.6 shows the dimensionless non-normalized moments as a function of center of mass energy, we see the variance σ^2 is increasing until $\sqrt{s} = 5$ GeV and then turn around decreasing with beam energy that mean the dynamical cumulants of the sigma field are much increasing compared with the equilibrium values, after the fireball evolves across the first order phase transition. Probing the non-Gaussian fluctuation is obtained by the non-vanishing skewness $S\sigma$ increasing with beam energy close to 1 around $\sqrt{s} = 20$ GeV. Finally, the kurtosis $\kappa\sigma^2$ has been shown the monotonic behavior within error bars, and sign change at beam energy $\sqrt{s} \sim 3$ GeV. The result give strong negative values of the kurtosis at second hit corresponding to the first order phase transition described in (M. A. Stephanov, 2011). Due to the trajectories passing through the first-order phase transition cross the freeze-out curve twice, we then connect them together to obtain a range of possible cumulant values for the lowest beam energies. Consider energy curve on gray band, the variance, which is less sensitive, decreases by a factor of 2 after passing through the second crossing. A memory effect found on the skewness, though somewhat less dramatic. The most sensitive susceptibility is seen in the kurtosis. We found that the kurtosis is dropping to a value -5 .

5.6 Comparison with experimental data

Experimentally, it has been measured the fluctuation of the net-proton. Especially, the $S\sigma$ and $\kappa\sigma^2$ has been investigated as shown in Figure 5.7.

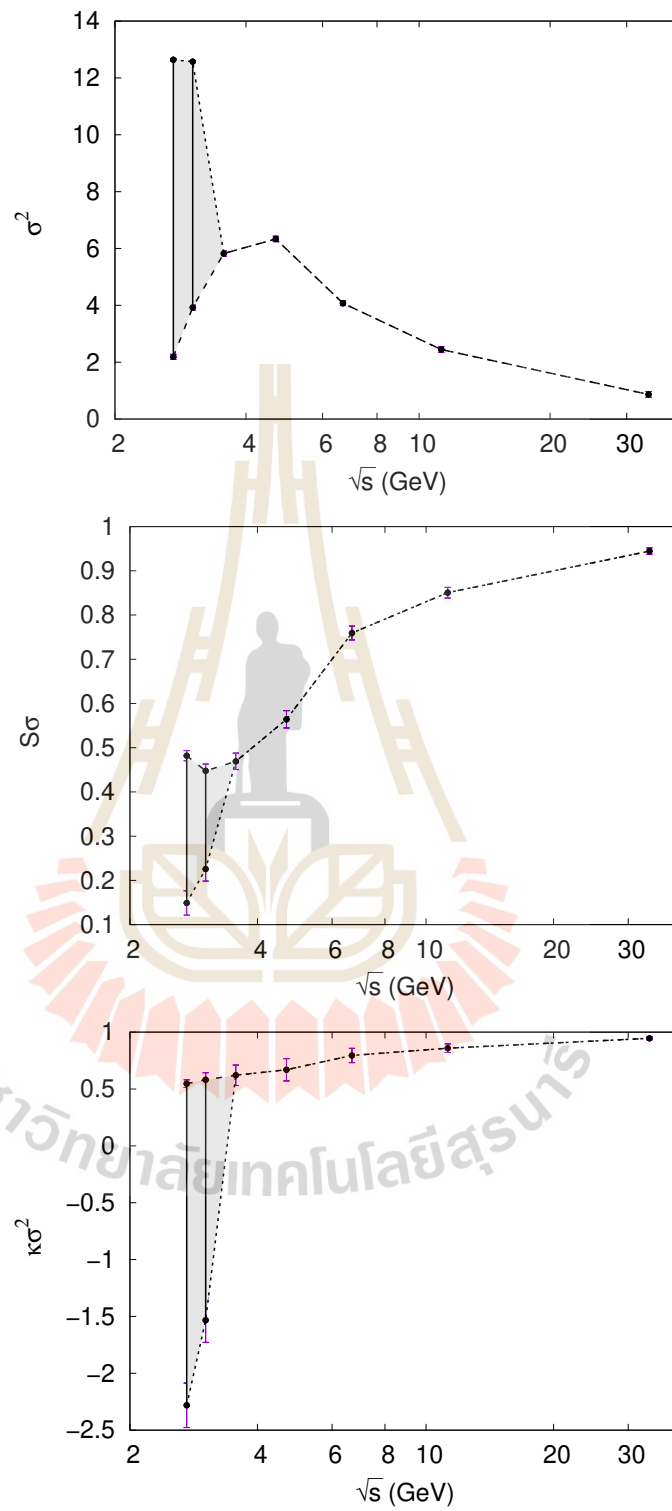


Figure 5.6 The fluctuation of net-proton is shown in ratio of high moment such σ^2 , $S\sigma$ and $\kappa\sigma^2$ as a function of center of mass energy \sqrt{s}

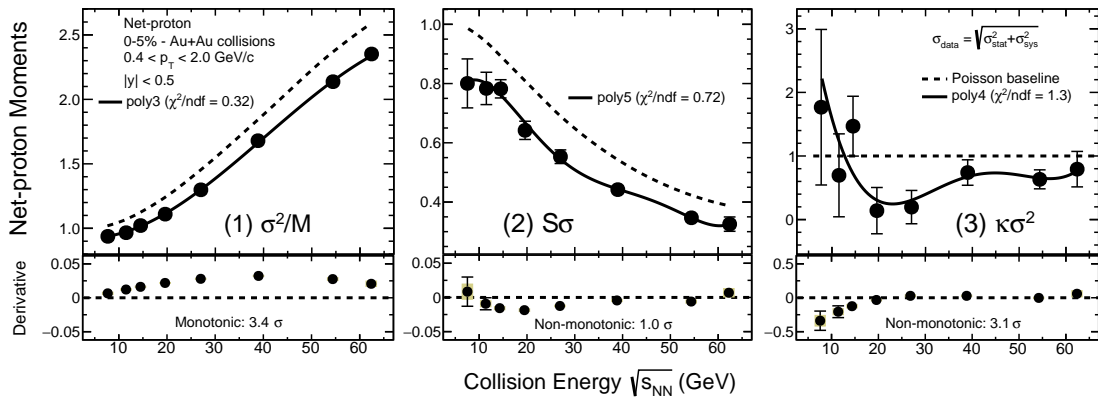


Figure 5.7 (1) σ^2/M , (2) $S\sigma$ and (3) $\kappa\sigma^2$ of net-proton distributions for 0-5% central Au+Au collisions from $\sqrt{S_{NN}} = 7.7 - 62.4$ GeV measured by STAR (STAR Collaboration et al., 2021).

As shown in Figure 5.7, We see that the net-proton fluctuation for 0-5% central Au+Au collisions fit to a polynomial approximation. The left panel σ^2/M is fitting with a polynomial of order 3 and its local derivative of polynomial fit with respect to collision energy is increasing monotonically. The middle $S\sigma$ is fitting with a polynomial of order 5 and its local derivative of polynomial fit have non-monotonic behavior. The right panel $\kappa\sigma^2$ is fitting with a polynomial of order 4 and its local derivative of polynomial fit is increasing monotonically. Moreover we found the negative sign changed of $\kappa\sigma^2$ at low energy. Thus we see clearly that the cumulant ratios as a function of beam energy change from a monotonic variation to a non-monotonic variation with higher orders. To compare with experimental data, we measure the fluctuation of the net-proton number. On the variance σ^2 , the nonmonotonic behavior is observed, but the STAR experiment obtain monotonically increasing. If we consider at low energy, our result is corresponding to STAR. On the skewness $S\sigma$, we see the fluctuation is converge to the Poisson base line that is observed on both of STAR and our result. But our skewness is increasing monotonically different from STAR decreasing monotonically. The most dramatic kurtosis $\kappa\sigma^2$ is increasing monotonically. Although it increases monotonically within error bars on STAR experiment, we still see the negative sign change at low energy both

of them. This agreement could hint that the first order phase transition is observed at $\sqrt{s} = 3$ GeV.



CHAPTER VI

SUMMARY AND CONCLUSIONS

Currently, the higher-order multiplicity moments are one tool to locate the QCD critical point. The high energy physics hopes to pinpoint the one point that connecting the first order phase transition, distinguishing the quark gluon plasma created at low-medium from the hadronic medium.

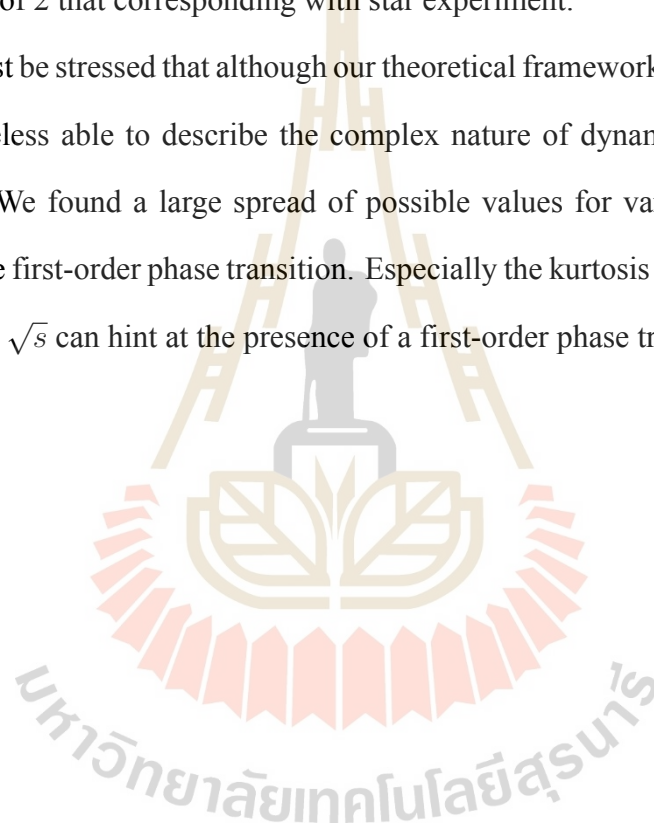
In this work, we focus on the dynamic of the sigma field (σ) as the order parameter on the chiral phase transition. The one phase has occurred in the expansion of the fireball to the hadronic matter described the spontaneous chiral symmetry breaking. The Langevin equation is described the evolution of the order parameter coupled with Bjorken's scaling picture including damping coefficient η and the stochastic noise $\xi(t)$ by White/Gaussian distribution.

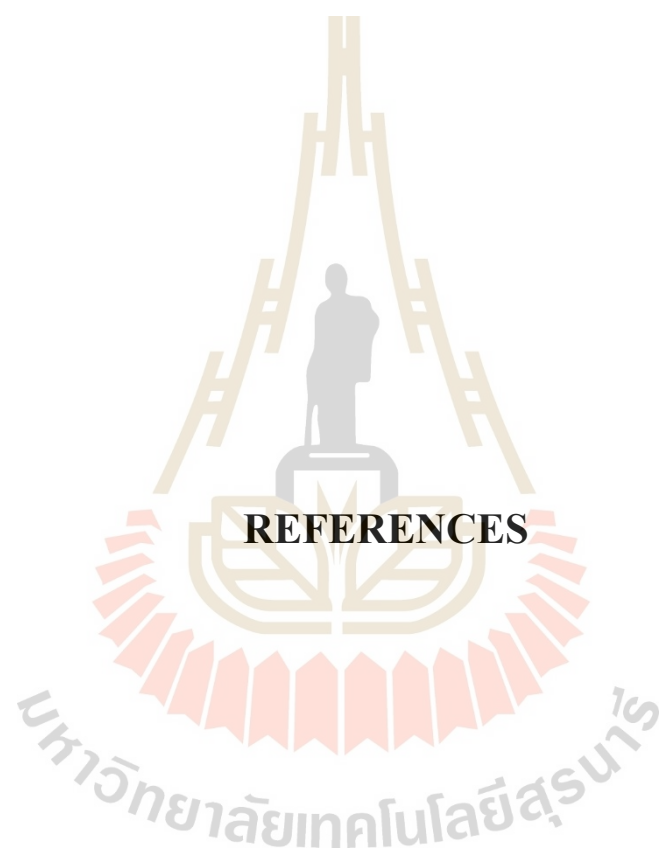
We study the fluctuation of the sigma field by solving the Langevin equation to investigate locating QCD critical point. The fluctuation of the sigma field is obtained by higher order moments. To compare with the experiment, we connect the fluctuation of sigma to proton given by the perturbation of effective mass.

We have studied cumulant ratios of the sigma field for different beam energies within the nonequilibrium chiral Bjorken model based on the quark-meson Lagrangian and observed double-crossing of the freeze-out curve leads to an increased range of possible cumulant values for the lowest beam energies. The kurtosis give a monotonically increasing with the beam energy. The most sensitive susceptibility found the strong negative values of the kurtosis of the order parameter and decreasing by a factor of 5. As argued in (M. A. Stephanov, 2011) are understood as a direct consequence of a first-order phase transition. For comparison with experimental data, we need to evaluate the

fluctuations in the net-proton number after a correct treatment of volume fluctuations and the possible need for an extension of the Lagrangian to cure the problem of negative pressure at lowest temperatures. We neglect the effect of the volume fluctuation. When we investigate on the higher cumulants of net proton, we find a monotonic behavior but the star experiment is observed nonmonotonic construction. Even the fluctuation behavior is not obey the experiment, we still see a negative value of kurtosis decreasing with a factor of 2 that corresponding with star experiment.

It must be stressed that although our theoretical framework is just a simple model it is nevertheless able to describe the complex nature of dynamical phenomena near a chiral CP. We found a large spread of possible values for variance, skewness, and kurtosis at the first-order phase transition. Especially the kurtosis with strongly negative values at low \sqrt{s} can hint at the presence of a first-order phase transition.





REFERENCES

REFERENCES

- Aggarwal, M. M., Ahammed, Z., Alakhverdyants, A. V., Alekseev, I., Alford, J., Anderson, B. D., Arkhipkin, D., Averichev, G. S., Balewski, J., and Barnby, L. S. (2010). Higher Moments of Net Proton Multiplicity Distributions at RHIC. **Physical Review Letters** 105(2).
- Alford, M., Rajagopal, K., and Wilczek, F. (1998). QCD at finite baryon density: nucleon droplets and color superconductivity. **Physics Letters B** 422(1-4): 247–256.
- Andronic, A., Braun-Munzinger, P., and Stachel, J. (2006). Hadron production in central nucleus–nucleus collisions at chemical freeze-out. **Nuclear Physics A** 772(3-4): 167–199.
- Aoki, Y., Endrődi, G., Fodor, Z., Katz, S. D., and Szabó, K. K. (2006). The order of the quantum chromodynamics transition predicted by the standard model of particle physics. **Nature** 443(7112): 675–678.
- Bjorken, J. D. (1983). Highly relativistic nucleus-nucleus collisions: The central rapidity region. **Physical Review D** 27(1): 140.
- Cassol-Seewald, N. C. and Krein, G. (2007). Numerical simulation of Ginzburg-Landau-Langevin equations. en. **Brazilian Journal of Physics** 37: 37–40.
- Cassol-Seewald, N., Farias, R., Fraga, E., Krein, G., and Ramos, R. O. (2012). Langevin simulation of scalar fields: Additive and multiplicative noises and lattice renormalization. **Physica A: Statistical Mechanics and its Applications** 391(16): 4088–4099.
- Cheng, M., Hegde, P., Jung, C., Karsch, F., Kaczmarek, O., Laermann, E., Mawhinney, R. D., Miao, C., Petreczky, P., and Schmidt, C. (2009). Baryon number, strangeness,

- and electric charge fluctuations in QCD at high temperature. **Physical Review D** 79(7).
- Cleymans, J., Oeschler, H., Redlich, K., and Wheaton, S. (2006). Comparison of chemical freeze-out criteria in heavy-ion collisions. 73(3), 034905: 034905. arXiv: hep-ph/0511094 [hep-ph].
- Fehling, D. (2008). The standard model of particle physics: A lunchbox's guide. **The Johns Hopkins University**, Retrieved on: 12–03.
- Gavai, R. V. and Gupta, S. (2008). QCD at finite chemical potential with six time slices. **Physical Review D** 78(11).
- Herold, C. (2013). Signals for the QCD Phase Transition in Nonequilibrium Chiral Fluid Dynamics. PhD thesis.
- Herold, C., Bleicher, M., Nahrgang, M., Steinheimer, J., Limphirat, A., Kobdaj, C., and Yan, Y. (2018). Broadening of the chiral critical region in a hydrodynamically expanding medium. **The European Physical Journal A** 54(2).
- Herold, C., Kittiratpattana, A., Kobdaj, C., Limphirat, A., Yan, Y., Nahrgang, M., Steinheimer, J., and Bleicher, M. (2019). Entropy production and reheating at the chiral phase transition. **Physics Letters B** 790: 557–562. arXiv: 1810.02504 [hep-ph].
- Herold, C., Nahrgang, M., Mishustin, I., and Bleicher, M. (2013). Chiral fluid dynamics with explicit propagation of the Polyakov loop. **Physical Review C** 87(1).
- Kittiratpattana, A. (2017). ENTROPY PRODUCTION AT THE CHIRAL PHASE TRANSITION. MA thesis. Suranaree University of Technology.
- Koch, V. (1997). Aspects of Chiral Symmetry. **International Journal of Modern Physics E** 6(2): 203–249. arXiv: nucl-th/9706075 [nucl-th].
- Landau, L. (1953). Collected Papers, No. 88. **Izv. Akad. Nauk, Ser. Fiz** 17: 51.
- Luo, X. (2012). Error Estimation for Moments Analysis in Heavy Ion Collision Experiment. **Journal of Physics G** 39: 025008. arXiv: 1109.0593 [physics.data-an].

- Monnai, A. (2014). **Relativistic Dissipative Hydrodynamic Description of the Quark-Gluon Plasma**. Springer Science & Business Media.
- Nahrgang, M., Herold, C., and Bleicher, M. (2013). Influence of an inhomogeneous and expanding medium on signals of the QCD phase transition. **Nuclear Physics A** 904-905: 899c–902c.
- Nahrgang, M., Leupold, S., Herold, C., and Bleicher, M. (2011). Nonequilibrium chiral fluid dynamics including dissipation and noise. **Physical Review C** 84(2).
- Ollitrault, J.-Y. (2008). Relativistic hydrodynamics for heavy-ion collisions. **European Journal of Physics** 29(2): 275.
- Schmidt, H. and Schukraft, J. (1992). The physics of ultra-relativistic heavy-ion collisions. **NUCLEAR PHYSICS AND RADIATION PHYSICS (G3450)** 23(GSI-92-19(PREPR.)): 142.
- Shi, S. and collaboration, S. (2009). Event anisotropy ν_2 at STAR. **Nuclear Physics A** 830(1-4): 187c–190c.
- Sinha, B. (2016). Cold dark matter and the cosmic phase transition. **Journal of Physics: Conference Series** 668: 012028.
- STAR Collaboration, Abdallah, M. S., Adam, J., Adamczyk, L., Adams, J. R., Adkins, J. K., Agakishiev, G., Aggarwal, I., and Aggarwal, M. M. (2021). Cumulants and Correlation Functions of Net-proton, Proton and Antiproton Multiplicity Distributions in Au+Au Collisions at RHIC. **arXiv e-prints**, arXiv:2101.12413: arXiv:2101.12413. arXiv: 2101.12413 [nucl-ex].
- Steinbrecher, P. (2019). The QCD crossover at zero and non-zero baryon densities from Lattice QCD. **Nuclear Physics A** 982: 847–850.
- Stephanov, M., Rajagopal, K., and Shuryak, E. (1998). Signatures of the Tricritical Point in QCD. **Physical Review Letters** 81(22): 4816–4819.

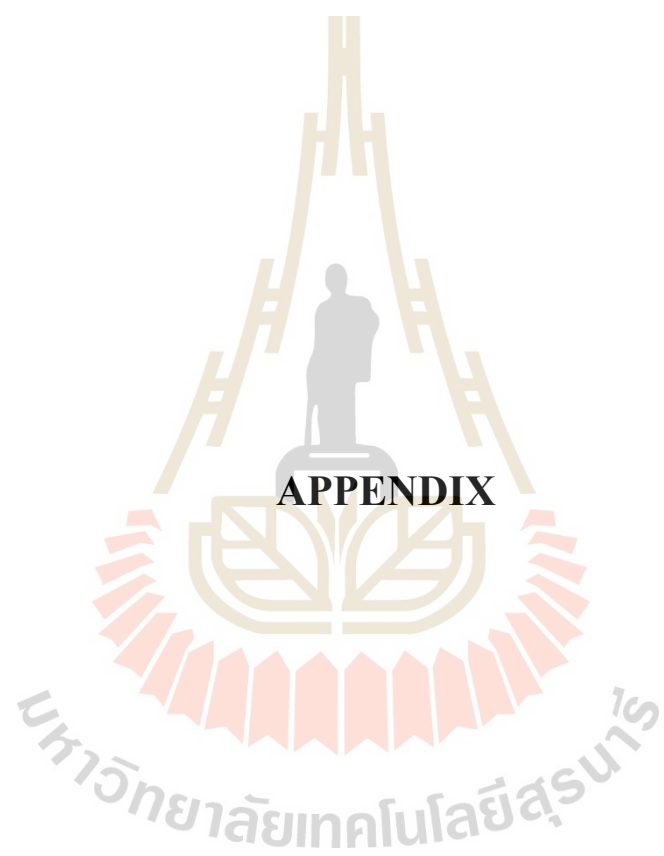
Stephanov, M. A. (2009). Non-Gaussian Fluctuations near the QCD Critical Point.

Physical Review Letters 102(3).

Stephanov, M. A. (2011). Sign of Kurtosis near the QCD Critical Point. **Physical Review**

Letters 107(5).





APPENDIX

APPENDIX

UNIT AND NOTATIONS

We work in units where $c = h = k_B = 1$. With the relations

$$x = ct, \tag{1}$$

$$hk = p, \tag{2}$$

$$E = k_B T, \tag{3}$$

In particle physics, the space x and time t and momentum p as well as energy E and temperature T are all in the same dimensions i.e. fm (femtometer or fermi) and MeV (mega electron volt) respectively. These two are also equivalent and can be transformed into each other via

$$1 = hc = 197.3 \text{ MeVfm} \tag{4}$$

The relations to usual SI-units are $1 \text{ fm} = 10^{-15} \text{ m}$ and $1 \text{ MeV} = 1.602 \cdot 10^{-13} \text{ J}$. The constants are the speed of light $c = 2.99792458 \cdot 10^8 \text{ m/s}$, the Planck constant $h = 1.055 \cdot 10^{-34} \text{ Js}$ and the Boltzmann constant $k_B = 1.381 \cdot 10^{-23} \text{ J/K}$.

In four-dimensional Minkowski space, we write contravariant four-vectors as

$$x^\mu = (t, x, y, z) \tag{5}$$

One can calculate the corresponding covariant vector $x_\mu = g_{\mu\nu}x^\nu$ from the met-

ric tensor $g_{\mu\nu}$ which we define in the convention

$$g_{\mu\nu} = \begin{pmatrix} 1 & 0 & 0 & 0 \\ 0 & -1 & 0 & 0 \\ 0 & 0 & -1 & 0 \\ 0 & 0 & 0 & -1 \end{pmatrix} \quad (6)$$

such that

$$x_\mu = (t, -x, -y, -z) \quad (7)$$

With this, the inner product

$$x^\mu x_\mu = t^2 - x^2 - y^2 - z^2 \quad (8)$$

is Lorentz invariant, a so-called Lorentz scalar. We define differential operators as

$$\partial_\mu = \frac{\partial}{\partial x^\mu} = \left(\frac{\partial}{\partial t}, \frac{\partial}{\partial x}, \frac{\partial}{\partial y}, \frac{\partial}{\partial z} \right), \quad \partial^\mu = \frac{\partial}{\partial x_\mu} = \left(\frac{\partial}{\partial t}, -\frac{\partial}{\partial x}, -\frac{\partial}{\partial y}, -\frac{\partial}{\partial z} \right) \quad (9)$$

One can multiply these two to obtain the Lorentz invariant d'Alembertian operator

$$\partial^\mu \partial_\mu = \frac{\partial^2}{\partial t^2} - \frac{\partial^2}{\partial x^2} - \frac{\partial^2}{\partial y^2} - \frac{\partial^2}{\partial z^2} \quad (10)$$

The energy-momentum four-vector of a particle in the contra- and covariant form reads

$$p^\mu = (E, \vec{p}), \quad p_\mu = (E, -\vec{p}) \quad (11)$$

with E the energy and \vec{p} the three-momentum of the particle. The square gives the invariant mass

$$p^\mu p_\mu = E^2 - \vec{p} \cdot \vec{p} = m^2 \quad (12)$$

The Dirac matrices are a set of four 4×4 matrices $\{\gamma^0, \gamma^1, \gamma^2, \gamma^3\}$ that were originally introduced by Dirac to transform the second-order Klein-Gordon equation into a first-order differential equation. The γ -matrices act on a space of spinors which are defined by their behavior under rotations. They obey the Dirac algebra, i.e. the anticommutation relation

$$\{\gamma^\mu, \gamma^\nu\} = \gamma^\mu \gamma^\nu + \gamma^\nu \gamma^\mu = 2g^{\mu\nu} \quad (13)$$

In the Dirac standard notation they have the form

$$\gamma^0 = \begin{pmatrix} 1 & 0 & 0 & 0 \\ 0 & 1 & 0 & 0 \\ 0 & 0 & -1 & 0 \\ 0 & 0 & 0 & -1 \end{pmatrix}, \quad \gamma^1 = \begin{pmatrix} 0 & 0 & 0 & 1 \\ 0 & 0 & 1 & 0 \\ 0 & -1 & 0 & 0 \\ -1 & 0 & 0 & 0 \end{pmatrix}, \quad (14)$$

$$\gamma^2 = \begin{pmatrix} 0 & 0 & 0 & -i \\ 0 & 0 & i & 0 \\ 0 & i & 0 & 0 \\ -i & 0 & 0 & 0 \end{pmatrix}, \quad \gamma^3 = \begin{pmatrix} 0 & 0 & 1 & 0 \\ 0 & 0 & 0 & -1 \\ -1 & 0 & 0 & 0 \\ 0 & 1 & 0 & 0 \end{pmatrix}$$

In addition, one often defines a fifth* γ -matrix as

$$\gamma^5 = i\gamma^0\gamma^1\gamma^2\gamma^3 = \begin{pmatrix} 0 & 0 & 1 & 0 \\ 0 & 0 & 0 & 1 \\ 1 & 0 & 0 & 0 \\ 0 & 1 & 0 & 0 \end{pmatrix} \quad (15)$$

with which one can define projectors P_L and P_R on the subspaces of particles with different chirality, left and right handed:

$$P_L = \frac{1 - \gamma^5}{2}, \quad P_R = \frac{1 + \gamma^5}{2} \quad (16)$$

Furthermore, the inclusion of a γ^5 matrix changes scalars to pseudoscalars as it changes sign under parity transformations, so $\bar{\psi}\psi$ is a scalar, while $\bar{\psi}\gamma^5\psi$ transforms as a pseudoscalar.

The Gell-Mann matrices T_a that occur in the QCD Lagrangian are the infinitesimal generators of the $SU(3)$ color gauge group. They form a Lie algebra obeying the commutation relations

$$[T^a, T^b] = T^a T^b - T^b T^a = i f^{abc} T^c \quad (17)$$

*It was called fifth because back then the γ^i were counted from 1 to 4, so it is reasonable to call a new one as fifth. But nowadays, we intuitively start with 0 instead

with the completely antisymmetric structure constants

$$f^{123} = 1, f^{147} = f^{165} = f^{246} = f^{257} = f^{345} = f^{376} = \frac{1}{2}, f^{458} = f^{678} = \frac{\sqrt{3}}{2} \quad (18)$$

The Gell-Mann matrices can be written as $T^a = \lambda^a/2$ with the 3×3 matrices

$$\lambda^1 = \begin{pmatrix} 0 & 1 & 0 \\ 1 & 0 & 0 \\ 0 & 0 & 0 \end{pmatrix}, \lambda^2 = \begin{pmatrix} 0 & -i & 0 \\ i & 0 & 0 \\ 0 & 0 & 0 \end{pmatrix}, \lambda^3 = \begin{pmatrix} 1 & 0 & 0 \\ 0 & -1 & 0 \\ 0 & 0 & 0 \end{pmatrix} \quad (19)$$

$$\lambda^4 = \begin{pmatrix} 0 & 0 & 1 \\ 0 & 0 & 0 \\ 1 & 0 & 0 \end{pmatrix}, \lambda^5 = \begin{pmatrix} 0 & 0 & -i \\ 0 & 0 & 0 \\ i & 0 & 0 \end{pmatrix}, \lambda^6 = \begin{pmatrix} 0 & 0 & 0 \\ 0 & 0 & 1 \\ 0 & 1 & 0 \end{pmatrix} \quad (20)$$

$$\lambda^7 = \begin{pmatrix} 0 & 0 & 0 \\ 0 & 0 & -i \\ 0 & i & 0 \end{pmatrix}, \lambda^8 = \frac{1}{\sqrt{3}} \begin{pmatrix} 1 & 0 & 0 \\ 0 & 1 & 0 \\ 0 & 0 & -2 \end{pmatrix} \quad (21)$$

CURRICULUM VITAE

NAME: PORAMIN SAIKHAM

GENDER: Male

NATIONALITY: Thai

DATE OF BIRTH: SEPTEMBER 25, 1994

E-MAIL: kob_poramin@hotmail.com

EDUCATIONS:

- 2007 - 2013, High school at Kalasinpittayasan school
- 2013 - 2017, Bachelor of Science, Physics department, Institute of science, Khonkaen University
- 2017 - 2020. Master of Science, School of Physics, Institute of Science, Suranaree University of Technology

EXPERIENCE:

- Participated in Academic Olympics at khonkaen University
- Participated in the Machine and Deep Learning Workshop at Suranaree University

SCHOLARSHIPS:

- Royal Thai Scholarship from the Development and Promotion of Science and Technology Talents Project (DPST)

HORNORS AND AWARDS:

- Ranked 3rd in the country in mathematics competitions